

Elucidation and Control of Self-assembled Structures of Patchy Colloidal Particles

野口, 朋寛

<https://hdl.handle.net/2324/2236021>

出版情報 : 九州大学, 2018, 博士 (理学), 課程博士
バージョン :
権利関係 :

Elucidation and Control of Self-assembled Structures
of Patchy Colloidal Particles

Tomohiro Noguchi

2019

To my family

Abstract

When a colloidal particle has heterogeneity in their physical / chemical properties on its surface, the surface-surface interaction between particles or a particle and an object becomes anisotropic. Such particles thus behave as “colloidal molecules” that bind to each other only at specific sites on their surface, exhibiting various types of condensed phases according to their anisotropy. These condensed phases are also nano-microstructures composed of colloidal particles as building blocks, having been utilized in nanotechnology as a novel pathway to design self-assembled structures. There have been extensive theoretical and numerical studies to elucidate the relationships between the anisotropy of colloidal molecules and their self-assembly or phase behavior. However, parameters characterizing the particle, such as the number and arrangements of the bonding sites and bonding energy, are enormous, and thus the relationships are far from being thoroughly elucidated. In particular, it is difficult to appropriately control the anisotropic structure and interaction of particles in experiments. The experimental studies are therefore strongly required from both academic and application fields. We therefore worked on experimentally controlling the interaction between one-patch particles by the anisotropy of the surface properties and elucidating the self-assembled structures with the anisotropic structure of the particles. One-patch particles are simplest colloidal molecules, having one distinctive region (patch) with different physical or chemical properties on its surface.

First, we used amphiphilic one-patch particles (Janus particle) having a hydrophilic and a hydrophobic hemisphere and investigated the structures formed in the particle-water-oil ternary system. The emulsification, i.e. stabilization of dispersed state of water in oil or *vice versa*, with Janus particles as surfactants has been investigated in several works. However, we observed and elucidated various self-assembled structures depending on amphiphilicity for the first time by our one-particle-level observations. When the volume of water was smaller than that of the particles, a capillary bridge of water bonded between the hydrophilic hemispheres of the Janus particles, and the particles formed rod-like micelle structures. When the volume of water was large, spherical emulsion droplets formed, and the mechanism of the structure formation was similar to that of Pickering emulsions by particles having a uniform surface prop-

erties. These structures reflected the amphiphilic structure of the particles and were found to be qualitatively similar to the micelles/emulsions of amphiphilic molecular systems. Furthermore, characteristic behaviors of colloidal particle systems appeared; the aggregation structures were solid-like in the sense that thermal fluctuation was not effective, and “ideal surface active behavior” in which all particles are adsorbed on the water-oil interface was observed.

Next, we aimed to control the anisotropy of DLVO interactions, which is the most fundamental interaction working between colloidal particles, as a technique to introduce anisotropy into various colloidal particle systems. DLVO interactions consists of van der Waals attraction working between the same materials and electric double layer repulsion derived from surface charge, and the attraction is very strong between metal surfaces. Therefore, when dielectric particles with metal patches are used, it is expected that selective adsorption will occur between the patches of particles and between the patch and the surface of a metal object. In our experiments, the attraction and repulsion were independently controlled by the thickness of the metal patch and by the surface electric potential of the patches, respectively. We succeeded in realizing a high adsorption selectivity in the particle dispersion system; the patchy particles were not adsorbed each other, and the metal patches were only adsorbed on the surface of a metal object. This selectivity induced a monolayer of patchy particles on the surface of large metal particles, which can be regarded as a solid dielectric layer preventing large particles from aggregation between them.

Our study elucidated the self-assembled structures of amphiphilic colloidal molecules by one-particle-level observation, and developed colloidal molecules whose anisotropic interaction inducing unique self-assembly can be tuned by the most typical and useful interaction in colloidal systems, i.e., DLVO interactions. The high surface activity of amphiphilic patchy particles has a great potential for applications and controlling DLVO interactions is useful for realizing experimental systems of colloidal molecules.

Contents

ChapterI	General introduction	8
1	Colloidal particles and their dispersions	8
2	Colloidal particles	9
2.1	Isotropic particles	9
2.2	Anisotropic particles	10
3	Structure formation of colloidal particles: Effect of anisotropy by patches	13
3.1	Phase behavior of isotropic particles	13
3.2	Phase behavior of patchy particles	14
4	Surface-surface interactions	14
4.1	Mesoscopic structure, its physical property and functionality	22
5	Motivations and purposes	25
5.1	Motivations	25
5.2	Purposes	26
5.3	Thesis outline	26
ChapterII	Elucidation of self-assembled structures in amphiphilic Janus particles-water-oil ternary system	28
1	Introduction	28
1.1	Pickering emulsions	28
1.2	Surface activity of amphiphilic Janus particles and Pickering emulsions with them	34
1.3	Differences and similarities between AJP and amphiphilic molecules .	36
1.4	Motivation and Purpose	38
2	Experimental section	38

2.1	Preparing AJP	38
2.2	Structure formation and observation	39
3	Results and Discussion	41
3.1	The aggregates and the change in structure	41
3.2	Detail of micelle-like cluster and the formation mechanism	43
3.3	Detail of spherical droplet and the formation mechanism	46
4	Summary and conclusion	53
ChapterIII Control of adsorption behavior of metal-patchy dielectric particles utilizing anisotropy in DLVO interaction		55
1	Introduction	55
1.1	DLVO interaction	55
1.2	DLVO interaction of metallodielectric particle	62
1.3	Motivation and purpose	63
2	Experimental section	64
2.1	Preparation of MDPs	64
2.2	Adsorption of MDPs to an Au-patterned substrate	65
2.3	Adsorption of MDPs to half Au-coated large particles	68
3	Results and discussion	69
3.1	Adsorption of MDPs to Au-patterned substrate	69
3.2	Adsorption of MDPs to thick Au films on large particles	73
4	Summary	75
ChapterIV Concluding remarks		76
Acknowledgment		78

Chapter I

General introduction

1 Colloidal particles and their dispersions

Colloidal particles are fine particles of ~ 10 nm to μm in size. There are various colloidal dispersion systems where colloidal particles are stably dispersed in gases, liquids, or solids. In such systems, the dispersed particles are called dispersoids, and the continuous phase is called dispersion medium. There are many colloidal dispersion systems around us. For example, when colloidal particles are solid and the dispersion medium is gas, liquid, and solid, the examples of the dispersions are smoke (aerosol), ink (suspension), and colored glass (solid sol), respectively (Figure 1). In addition, it is known that colloidal dispersions exhibit nonlinear responses to external stimuli since they possess large internal degrees of freedom due to the enormous number of colloidal particles. In other words, in a colloidal dispersion, not only the physical property and functionality of colloidal particles, e.g. color, light scattering ability, and catalytic ability, but also their dispersion states or self-assembled structures play important roles in the behavior and properties of the system. For example, when particles form a network structure and gel, the system exhibits elasticity, and when the particles are conductive, the system becomes conductive. In addition to the academic interest in the characteristic physical properties of colloidal dispersions around us, the study of colloidal particles and their dispersions has also been carried out for developing functional nano/microstructured materials.

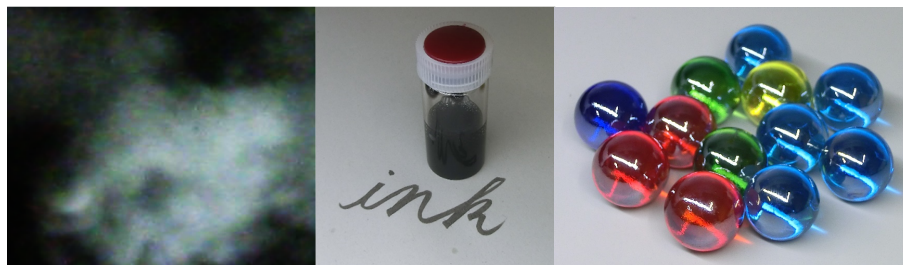


Figure 1. Examples of colloidal dispersions. From the left, smoke, ink, and colored glass.

2 Colloidal particles

2.1 Isotropic particles

Isotropic particles are those without anisotropy in e.g. shape and composition. There are various kinds of isotropic particles including core-shell particles, gel balls, even liquid droplets and more, but the most typical and widely used one is a hard sphere of homogeneous material compositions. Isotropic and spherical particles are also found in our daily life. For example, spherical colloidal particles are added to a foundation of cosmetic products in order to impart light scattering/irregular reflection ability, and to a road sign, where the particles are used to make its surface retroreflective (Figure 2). Isotropic monodisperse hard spheres have also been employed in theoretical and experimental studies. Colloidal dispersions are classified into a complex system because of the numerous internal parameters such as physical and chemical properties, volume fraction, and spatial arrangements of particles. Therefore, the use of the simplest colloidal particle, e.g. hard sphere, is useful for elucidating the fundamental and essential features of colloidal dispersions.



Figure 2. Application of spherical isotropic colloidal particles. Left; foundation, right; road sign.

2.2 Anisotropic particles

In nature, anisotropic colloidal particles and their dispersions are abundant (Figure 3). In recent years, studies on anisotropic particles have attracted attention of researchers in soft matter [1–4]. In particular, experimental studies have become more and more practical in this decade according to the development of particle fabrication techniques.

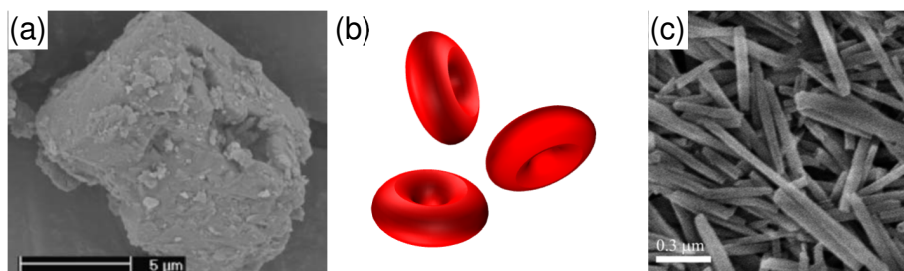


Figure 3. Examples of shape anisotropic particles. (a) A SEM image of a mineral dust particle found in a soil sample collected in northern Sahara [5]. (b) A schematic image of red blood cells. Their typical size is 7-8 μm . (c) A SEM image of halloysite clay particles [6].

The anisotropy of colloidal particles can be classified into two types; anisotropy in shape and substance (Figure 4) [1]. Anisotropy in substance is that in the spatial distribution of substance in one particle, and thereby such a particle has anisotropy in physical and/or chemical properties. These anisotropic particles show not only the anisotropy in the interaction but also active motion by consuming free energy by themselves (Figure 5) [7]. As described above, anisotropic colloidal particles exhibit essential difference from isotropic ones, and thus gain great attention from both experimental and theoretical points of view.

Figure 6 shows examples of shape-anisotropic particles [8]. There are variety of shapes from relatively simple ellipses and disk particles with different aspect ratios to complex polyhedral and branched particles.

As shown in Figure 4, it is possible to impart various types of anisotropy in physical / chemical properties by the anisotropy in substance, such as catalytic ability, amphiphilicity, conductivity, surface charge, color, etc.

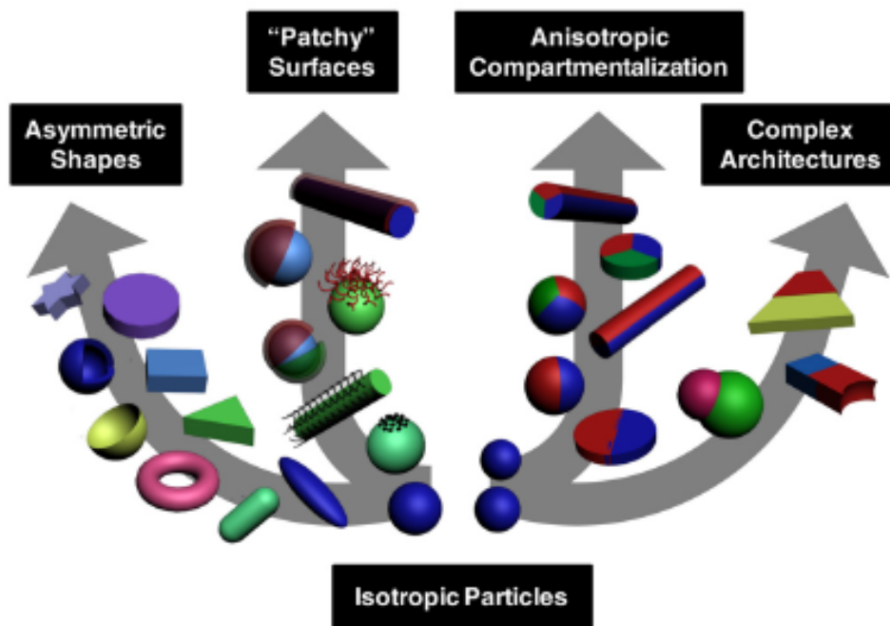


Figure 4. Various anisotropies in particles [1].

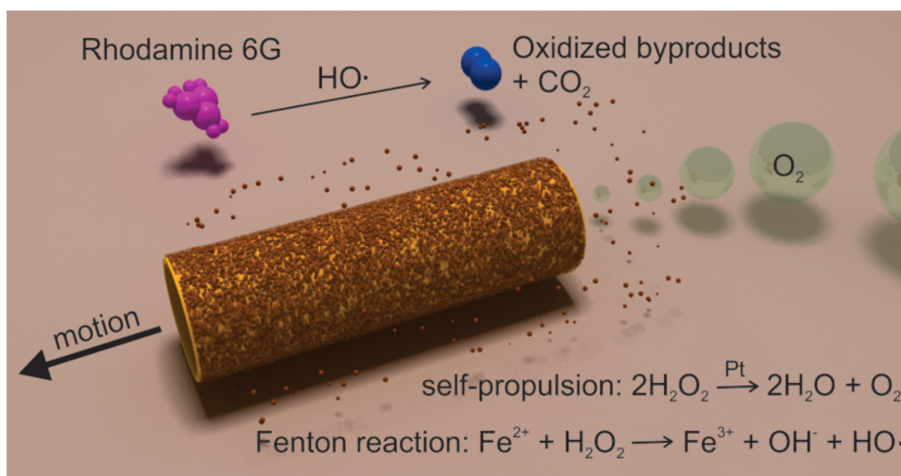


Figure 5. Schematic drawing of a catalytic tube particle self-propelling while decomposing H_2O_2 [7].

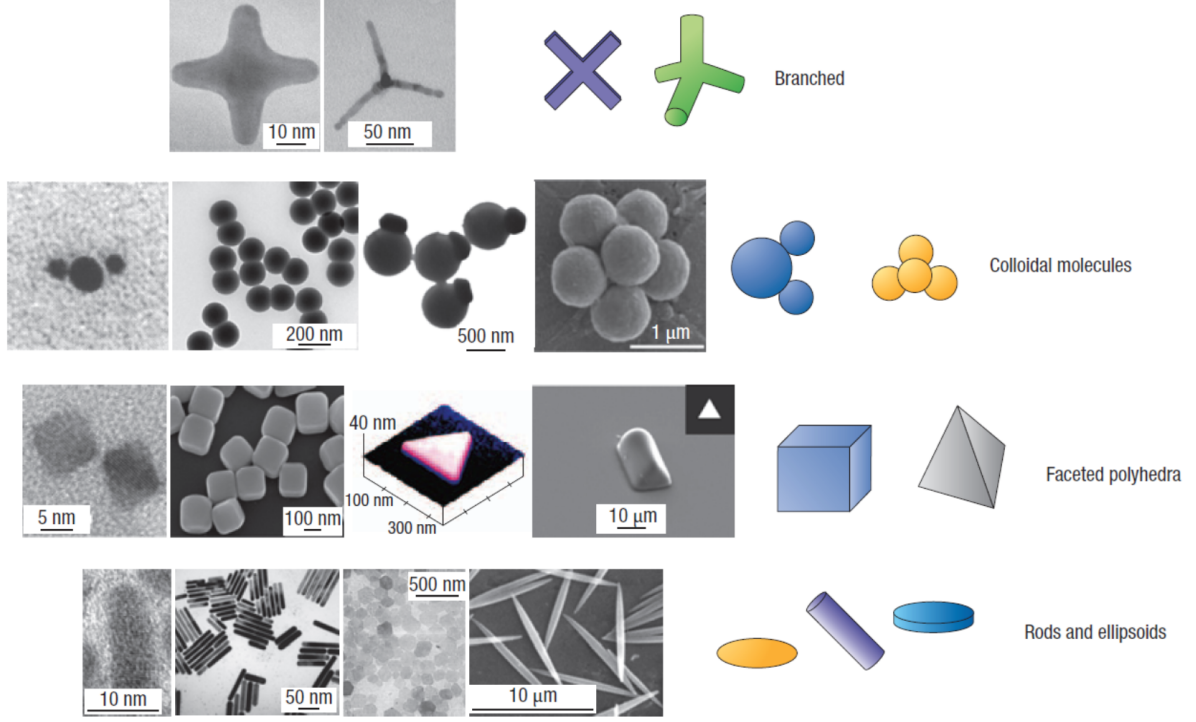


Figure 6. Various shape-anisotropic particles [8].

Patchy particles

Particles having distinctive regions (patches) with different physical / chemical properties on the particle surface are called patchy particles [9, 10]. Since the interaction between colloidal particles strongly depends on the properties of the particle surface, the anisotropy in the surface-surface interaction between patchy particles can be tuned by the patch. Patchy particles have been utilized in many theoretical studies of condensed phases, and various patchy particles have been experimentally realized. Various combinations of patchy anisotropic properties can be considered, such as hydrophilic-hydrophobic [11, 12], positive charge-negative charge [13], transparent-opaque [14], metal-dielectric [15], etc., inducing various anisotropic interactions depending on the properties of the patch and other surfaces. In addition, particles composed of multiple materials are called hybrid particles, being studied as functional nano particles for application [16].

3 Structure formation of colloidal particles: Effect of anisotropy by patches

The structures of aggregates formed by colloidal particles naturally depend on the interactions between them. Solid particles with shape anisotropy exhibit anisotropic hard-body interaction. Anisotropy of surface properties induces anisotropic surface-surface interaction in patchy particles. Due to these anisotropic interactions, anisotropic particles are expected to form characteristic structures which cannot be formed by isotropic particles. Therefore, by designing the anisotropic interaction between the particles, it is possible to obtain desired aggregated structures [16]. For example, attractively interacting patches, e.g. *sticky* patches [16], and the patches that bond to each other only for particular combinations of multiple patches [17], have been realized.

3.1 Phase behavior of isotropic particles

Colloidal particles exhibit thermal motion and thus can exhibit equilibrium phases in their condensed systems. A condensed system of colloidal particles has actually been used as a model experimental system to explore the phase behavior of general condensed systems. In condensed systems of isotropic particles, it is known that several phases appear depending on the interaction between particles, temperature, and volume fraction of particles (Figure 7). For example, monodispersed spherical particles only show face-centered-cubic and hexagonal close-packed structures as their crystalline phases in three dimensions. In addition, the interaction between particles is often sufficiently short-ranged (typically $\lesssim 10$ nm) compared with the particle size. When the interaction is short-ranged, no gas-liquid phase separation appears and particles crystalize from the fluid phase [18]. In addition, it is known that a glassy state appears in the condensed system when the particles are not monodisperse. Figure 7 shows the dependence of phase behavior on the volume fraction of particles [19].

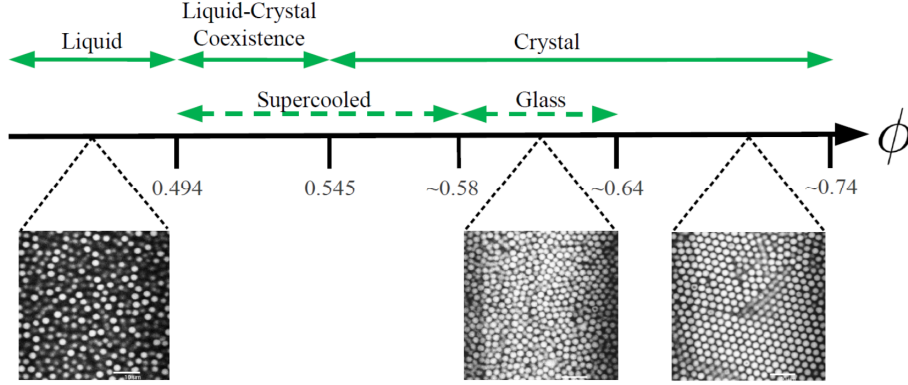


Figure 7. Phase behaviors of condensed systems of isotropic particles against particle density. ϕ is the volume fraction of particles. Solid green arrows indicate equilibrium states, and dashed arrows indicate metastable non-equilibrium states. Images are confocal micrographs of colloidal particle suspensions with 5% size dispersion [19].

3.2 Phase behavior of patchy particles

When a particle possesses sticky patches, number of binding sites (valence number), arrangements of them, and directions of bonds are limited in comparison with isotropic particles. Thus, such patchy particles are also called “colloidal molecules” [20,21]. In condensed systems of particles with sticky patches, various phase behaviors different from those of isotropic particles have been observed [22–28]. For example, as shown in Figure 8 (a-d), when a particle having tetrahedrally-arranged four patches, diamond crystal phase, body centered cubic phase, and gas-liquid phase separation appear, exhibiting complicated phase diagrams depending on the strength of the interaction and size of patches [29]. The phase diagram also depends on the valence number (Figure 8 (i)). In a two-dimensional system, as shown in Figure 9, triblock particles form a kagome lattice in the experiment [30].

4 Surface-surface interactions

Various interactions work between colloidal particles in a solvent depending on the physical / chemical properties of the particles and the solvent. The magnitude of the interaction is generally compared with thermal energy. Multiple types of interactions

4 SURFACE-SURFACE INTERACTIONS

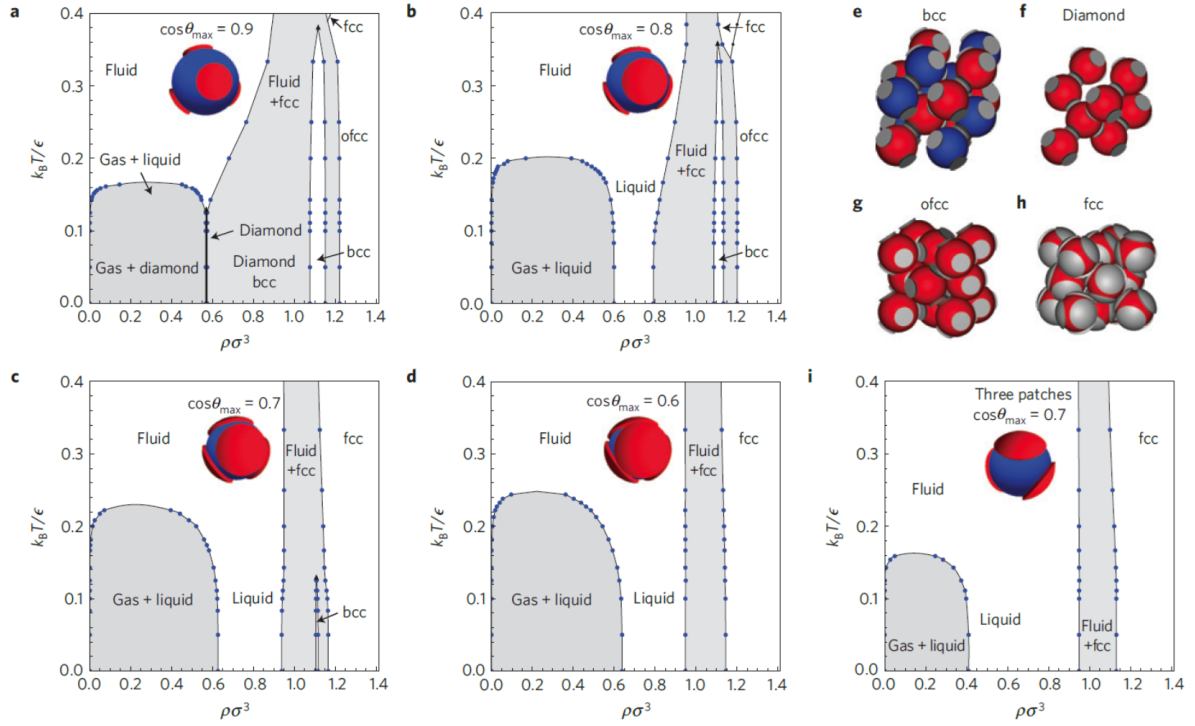


Figure 8. Phase diagrams of three- and four-patch particles, depending on the density, temperature, binding energy, width of binding sites, and the valence number [29].

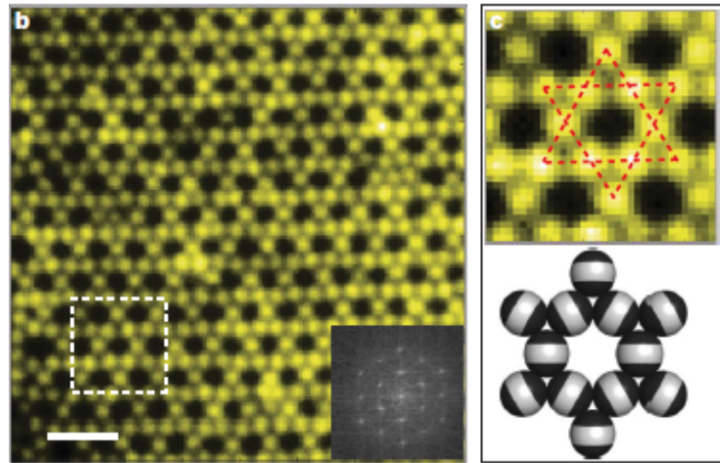


Figure 9. Fluorescence microscope image of a lattice formed by triblock (two-patches) particles, with its Fourier transformation image and schematic diagram. The scale bar is $4\ \mu\text{m}$ [30].

4 SURFACE-SURFACE INTERACTIONS

often work between particles.

Derjaguin-Landau-Verwey-Overbeek (DLVO) interactions

DLVO interaction is one of the most typical interactions considered and actually works in colloidal particles in an aqueous solution, and thus often used for discussing the dispersion stability and aggregation behavior of colloidal particles [18]. DLVO interaction is the sum of the repulsion by the electric double layer (EDL) produced by surface charge and the van der Waals (vdW) attraction between materials. A characteristic feature of DLVO interaction is that the potential profile against the interparticle distance drastically changes by the properties of particles and solvent. Figure 10 shows the scanning electron microscope and fluorescence microscope images of gold-polystyrene patchy particles and their clusters irreversibly aggregated by the vdW attraction between gold patches [31]. DLVO interaction is described in more detail in Sec.1.1 of Chapter III..

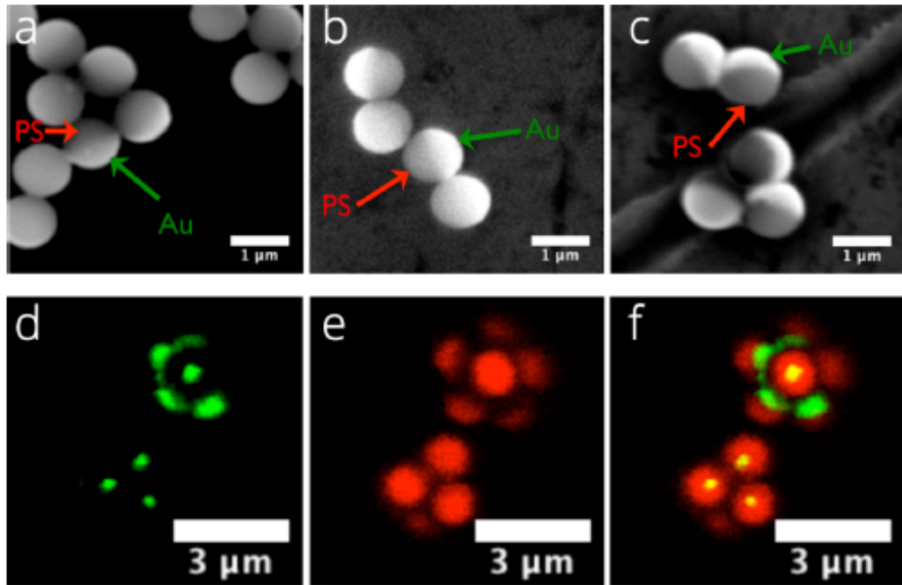


Figure 10. Gold-polystyrene patchy particles and their clusters. Green and red regions in (d-f) are gold patches and polystyrene surfaces, respectively [31].

Electrostatic interaction

An electrostatic interaction can be introduced between particles by modifying their surface by dissociable group. It is possible to impart not only positive or negative charge to a particle but also both positive and negative charges, i.e. a particle can be dipolar. Figure 11 shows the cluster formation of one-patch particles with a positively charged and negatively charged hemisphere in phosphate-buffered saline (PBS) buffer (pH: 6) with 1 mM ionic strength, together with the result of Monte Carlo simulations [13]. The cluster structures in the experiments (Column A) and in the simulations (Column B) agree, where the surfaces with the opposite sign, yellow hemisphere - red hemisphere, are adsorbed.

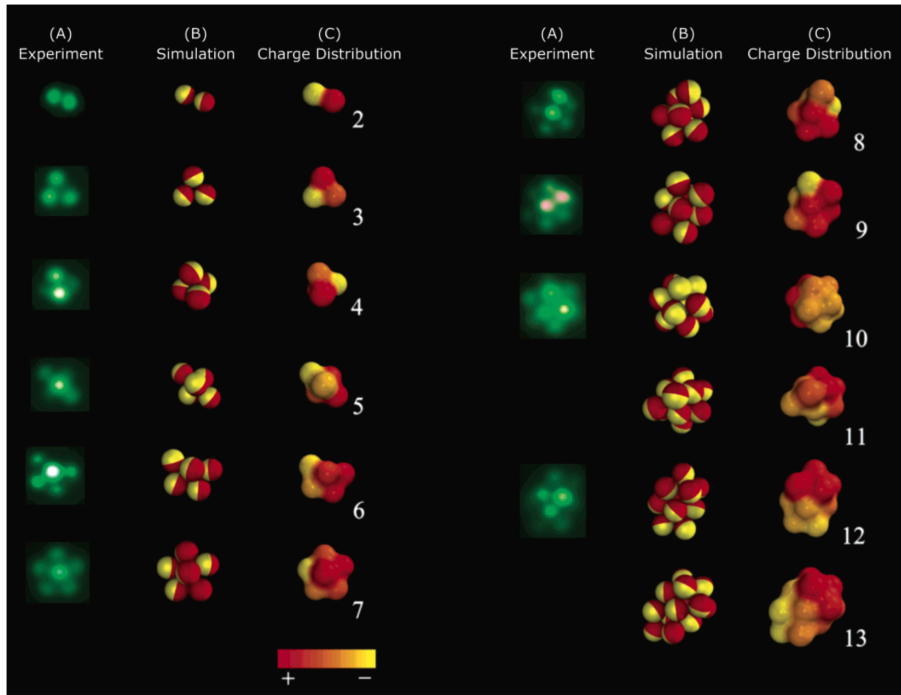


Figure 11. Clusters formed by charge dipolar particles in PBS buffer (pH: 6) with 1 mM ionic strength. Column A, column B, and column C are the epifluorescence observation images, the result of Monte Carlo simulations, and the charge distributions in the clusters of the B column. The numbers of particles constituting the clusters are shown in column C [13].

Hydrophilic / hydrophobic interaction

An attractive force works between hydrophobic surfaces in a polar solvent and between hydrophilic surfaces in an apolar solvent. These are called hydrophilic or hydrophobic interaction. Patches having the same hydrophilic / hydrophobic property attract each other, being sticky. Figure 12 shows the experimental results of the cluster formation of amphiphilic one-patch particles whose hydrophilic and hydrophobic surfaces are hemispherical and corresponding results of Monte Carlo simulations [32]. In the simulations, the yellow and blue hemispherical surfaces are the hydrophilic and hydrophobic surfaces, respectively. The particles showed a monomer state, small clusters, and long, branched wormlike strings at 0, 1, and 5 mM of KNO_3 concentrations, respectively.

Capillary interaction

When two particles are bridged by a small liquid droplet wetting their surfaces, an attractive (capillary) interaction occurs due to the interfacial tension of the droplet. This attraction is generally very strong compared with the vdW attraction at the scale of colloidal particles. When the liquid of a droplet is polar / apolar, the droplet prefers to wet hydrophilic / hydrophobic surfaces, and therefore the attraction is large between the surface of similar hydrophilicity. Figure 13 is an experiment in which three-dimensional clusters of amphiphilic one-patch particles are formed by the wetting-induced interaction [33]. Droplets of the polar phase are formed by the phase separation of binary liquid mixture (water - 2,6-lutidine). The droplets can wet only the hydrophilic hemispheres of the one-patch particles (the white hemisphere). When the volume of the polar phase decreases, clusters in which the hydrophilic surfaces of the particles face each other are formed (Figure 13 (a)). Figure 13 (b) shows optical microscope images of the cluster formation process and its schematic diagram. Figure 13 (c) shows optical microscope images of clusters of various numbers of particles.

Interaction induced by solvent criticality

An attractive interaction works between the hydrophilic or hydrophobic particles in the vicinity of the critical demixing point of a solvent between the polar and apolar phases. When the binary liquid mixture solvent is in the one phase region near the

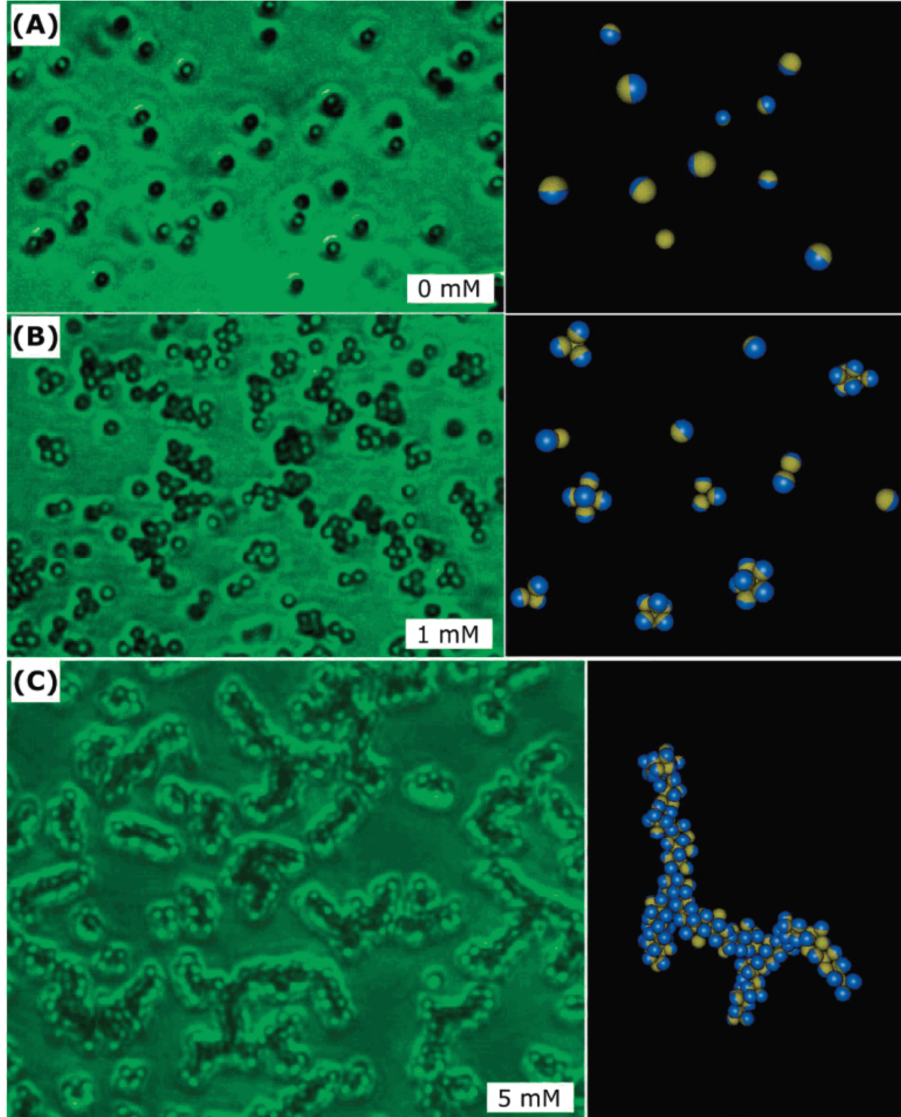


Figure 12. Aggregate structures formed by amphiphilic patchy particles in KNO₃ aqueous solution [32]. The left and right panels are epifluorescence observation images and simulation results, respectively.

critical demixing point, the composition of the solvent at the particle surface is biased so that the ratio of the liquid component having high affinity to the particle surface becomes high. In addition, the concentration fluctuation between the particles is spatially limited. These effects cause an attractive interaction between the surfaces of the same polarity. Figure 14 shows the aggregate structures of one-patch particles having a moderate and highly hydrophilic hemispherical surface near the critical point

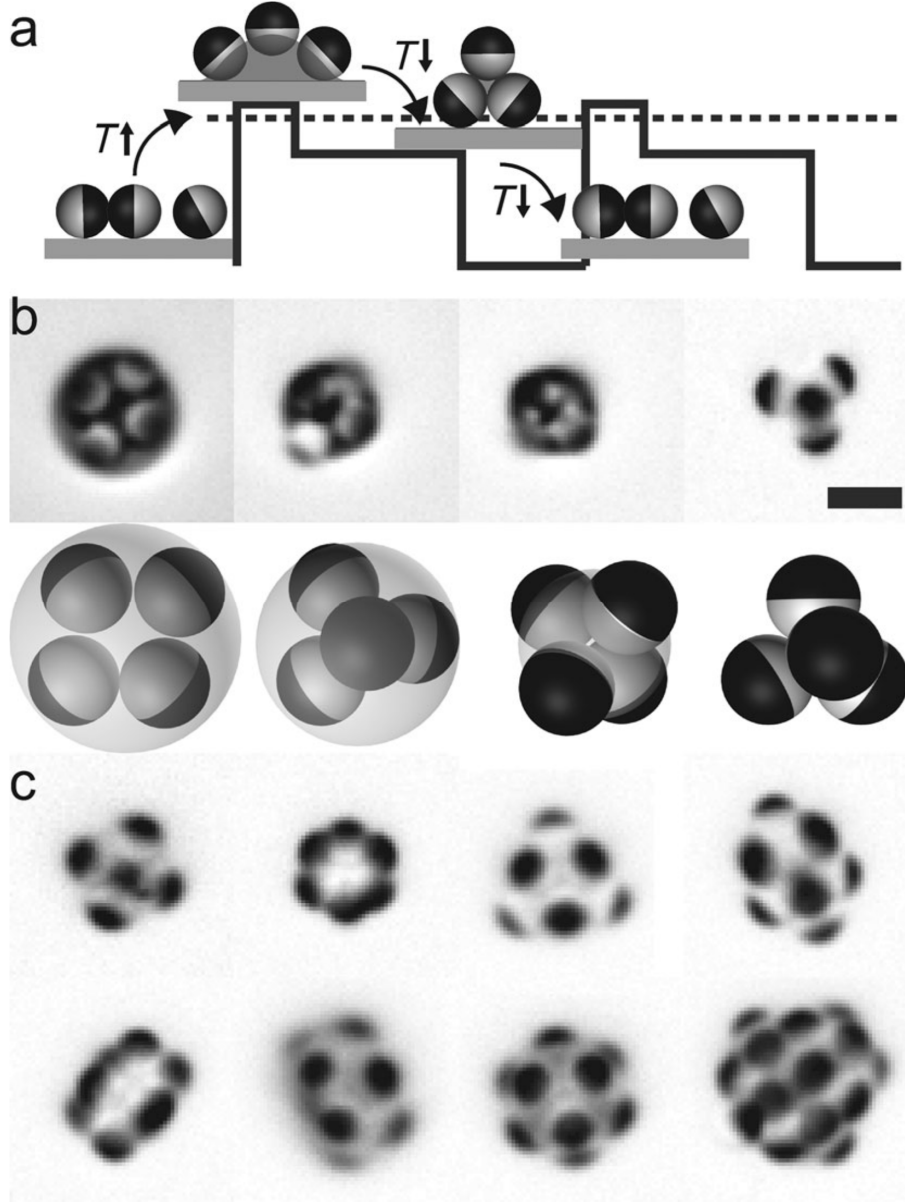


Figure 13. Three dimensional cluster formation of amphiphilic one-patch particles utilizing the phase transition of water - 2,6-lutidine binary mixture. The black and the white hemispheres of the particle are the hydrophobic and hydrophilic hemisphere, respectively. (a) A schematic drawing of the process forming and resolving clusters of the particles with the phase transition of solvent. (b) Optical and schematic images of the 4-particle cluster in the process of internal phase dissolving. Scale bar is $5 \mu\text{m}$. (c) Three-dimensional clusters formed by many particles [33].

4 SURFACE-SURFACE INTERACTIONS

of a binary liquid mixture (water - 2,6-lutidine) [34]. As the temperature approaches the critical point (Figure 14 (a) to (d)), the particles, first in a dispersed state (Figure 14 (a)), form trimers or tetramers (Figure 14 (b)), and then form tetramer chain structures (Figure 14 (c)). In the structures, the highly hydrophilic hemispherical surfaces (black surfaces) are adsorbed each other, and the structural development with temperature is driven the increase of attraction with approaching the critical point. In Figure 14 (d), which is very close to the critical point, the white hemispheres are also adsorbed each other and form a network structure.

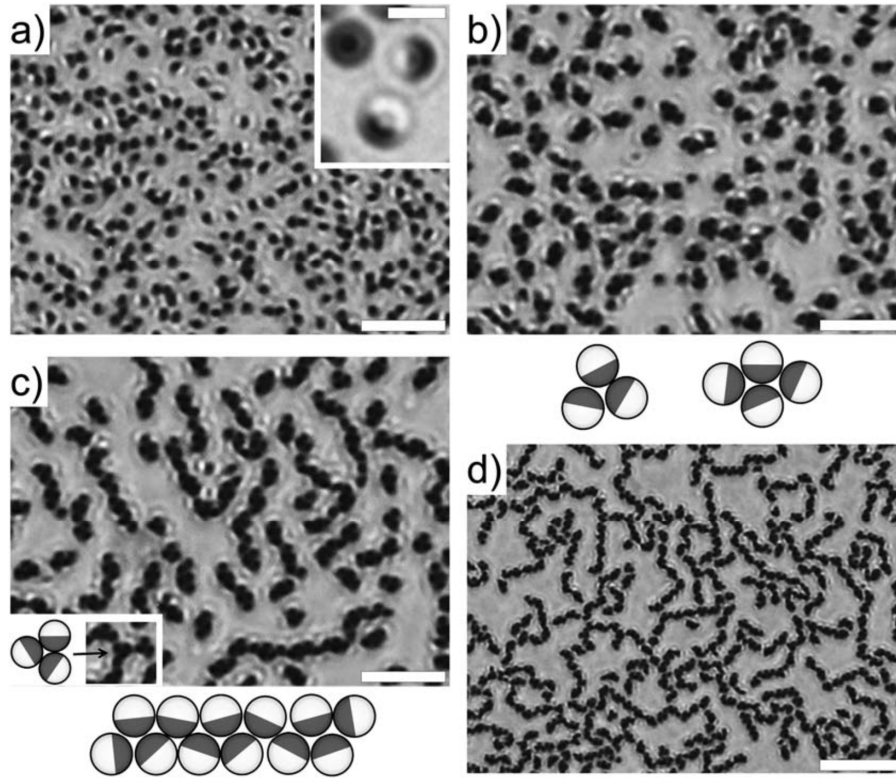


Figure 14. Temperature dependence of the aggregate structures formed by one-patchy particles composed of moderate and highly hydrophilic hemispheres near the critical demixing point of water - 2,6-lutidine binary mixture. The temperature differences from the critical point are -0.5, -0.2, -0.1, and -0.01 K respectively from (a) to (d). The scale bars are 2 μm in the inset in (a), 20 μm in (d), and 10 μm for the others [34].

Depletion interaction

In a system in which colloidal particles and non-adsorptive macromolecules are dispersed, an entropy-driven attractive interaction, depletion interaction, works between the particles. This interaction is generally weak, but it can be a dominant interaction in colloidal dispersions. Figure 15 is a schematic diagram of the key (red) and lock (green) particles, and an optical microscope image in an aqueous solution of poly ethylene oxide with a molecular weight of 600,000 [35]. Figure 15 (a) shows the region in which the polymers are excluded and the overlap of the excluded space of the key and lock particles, respectively. When the curvature of the key particle and that of the lock particle are exactly the same, the overlap of the excluded volumes, and thus the depletion interaction, is maximized. Figure 15 (b) shows the combining process of a key and lock particle; key particles entering the key hole of the lock particle are bound (green arrow), but key particles are not bound to the other part (red arrow). Figure 15 (c) shows the process in which a coupled key-lock particles combines with another lock particle.

Specific binding by DNA ligand

DNA chains are representative molecules having specificity in their binding target defined by the sequence of bases. By modifying two patches, A and B, with DNA chains having complementary single strand, selective binding between A and B patches are realized. Figure 16 shows the aggregated structures formed by particles having complementary A and B patches [36]. The left column presents optical microscope images of the aggregated structures, the middle column fluorescence microscopic images, and the right column schematic diagrams of the aggregation structures. A and B patch are selectively adsorbed, and various structures are formed depending on the arrangement of the patches.

4.1 Mesoscopic structure, its physical property and functionality

The characteristic length scale of the internal structure in a colloidal dispersion is naturally mesoscopic because of the particle size. In different from the structures with microscopic length scale, i.e. structures composed of atoms or molecules, and those

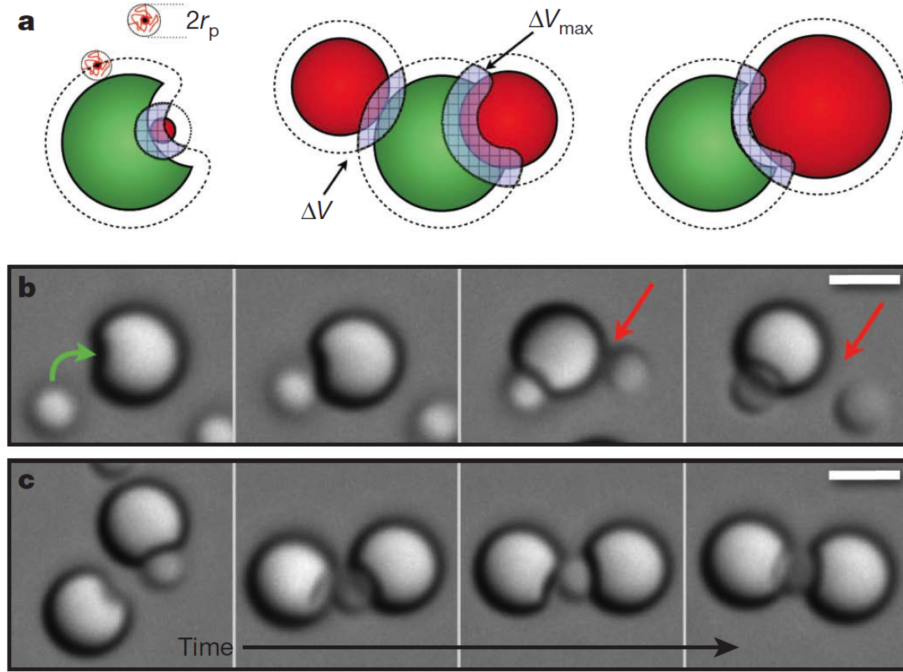


Figure 15. Schematic drawing and optical microscope images of the combination of key and lock particles in aqueous solution of poly ethylene oxide with a molecular weight of 600,000. The red and green particles in (a) are key and lock particles, respectively. The scale bar is $2 \mu\text{m}$ [35].

with macroscopic length scale around us, these structures with mesoscopic length scale exhibit characteristic features; the drastic increase in surface area compared with macroscopic structures, a relatively easy-change of internal structures in response to external input compared with microscopic structures, etc. These features induce unique physical properties and functionalities. For example, changes in the internal network structure give frequency dependence of viscoelasticity. The drastic increase in surface area dramatically increases the catalytic ability. In addition, mesoscopic structures often have a characteristic length in the order of visible light wavelength and thus exhibit characteristic optical properties such as absorption and reflection of light with specific wavelength. It is therefore expected that self-assembled structures of patchy particles can contribute to the creation of highly functional mesostructured materials [37].

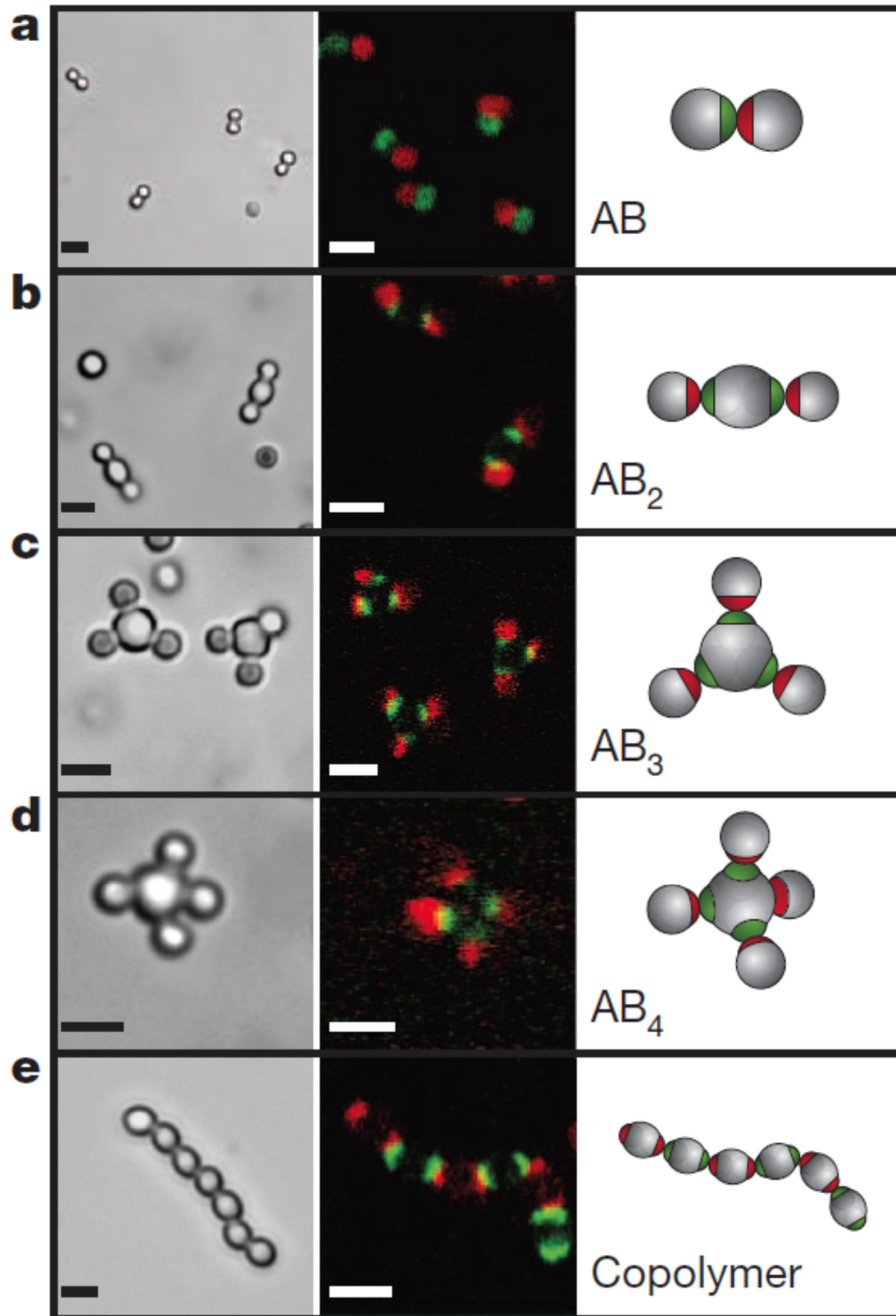


Figure 16. Aggregation structure of patchy particles with complementary DNA ligands. The scale bar is $2\ \mu\text{m}$ [36].

5 Motivations and purposes

5.1 Motivations

Patchy particles have extensive parameter space as colloidal molecules, such as the number and arrangements of bonding sites and the strength of bonds. Thus, the whole aspects of the role of the patchy surface anisotropy is not elucidated. Theoretical and numerical studies of condensed systems of patchy particles have greatly advanced in these decades because of the improvement of simulation methods and performance of computers [38–44]. In contrast, experimental studies are still advancing; it is not easy to appropriately control the anisotropic structure and interaction of particles in a real system. Deeper understanding of patchy particles in real, experimental systems is therefore strongly required from both academic and application point of view. We are therefore interested in the two following research themes.

Spherical amphiphilic one-patch particles have one hydrophilic and another hydrophobic region on the surface. Since this particle has qualitatively the same structure as a simple amphiphilic molecule, it is expected to have high surface activity and emulsification ability, stabilizing dispersion state of immiscible liquids such as water and oil. In addition, since various self-assembled structures and their ordered phases are known to appear in amphiphilic molecular dispersion systems in water or a water-oil mixture, similar structures and phases are expected to be formed in amphiphilic patchy particle systems. Nevertheless, such studies with amphiphilic patchy particles have not been reported, and self-assembled structures and their formation mechanisms are still to be elucidated. Clarification of these fundamental behaviors of patchy particles as surface active agents would contribute not only to their use as a superior and/or unique surfactant compared to surfactant molecules, but also to their application to designing self-assembled functional mesostructures.

In order to realize anisotropic bonding between patchy particles, various interactions have been utilized as described above. However, there are few researches introducing anisotropy to DLVO interaction of patchy particles and controlling their self-assembly with it, though DLVO interaction is the most fundamental one working between colloidal particles. When controlling anisotropy of DLVO interaction is realized, the

method would be a more universal one enabling the introduction of anisotropic interaction to various experimental systems of colloidal particles compared with the other methods introducing the other types of interactions described above. Our method would thus be useful for various fundamental studies with colloidal molecules and applications for producing functional nanostructures by patchy particles.

5.2 Purposes

In order to elucidate self-assembled structures and their formation mechanisms in amphiphilic patchy particle dispersion systems, we carried out experiments on the structure formation in amphiphilic Janus particles-water-oil ternary systems. Amphiphilic Janus particle is the simplest and symmetrical amphiphilic patchy particle composed of a hydrophilic hemisphere and a hydrophobic hemisphere, and thus it is suitable for capturing the essential features of their self-assembly. The details of the aggregation structures formed in this ternary system were observed at one-particle level, and the formation mechanisms were discussed with the typical interactions working in such particle-water-oil mixtures.

In order to realize the control of anisotropic DLVO interaction using patchy particles, the dependence of the adsorption behavior of metallodielectric particles to metal surface and dielectric surface on salt concentration was investigated. A metallodielectric particle is a type of patchy particle whose particle surface is composed of a metal and a dielectric part. We introduced the anisotropy in DLVO interaction to the system by tuning the repulsion by the surface charge of a patch and the strong vdW attraction by the thickness of a patch. The dependence of the adsorption behavior on the experimental conditions was studied with a flat dielectric substrate possessing thick metal films, and the self-assembly was observed with a freely dispersed large particle possessing a thick metal film.

5.3 Thesis outline

In Chapter II, we first describe the surface activity and self-assembly of colloidal particles and surfactants. Next, our fabrication method of amphiphilic one-patch (Janus) particles and experimental method are described. Then, the results of the

self-assembled structures in the amphiphilic Janus particles-water-oil ternary system explored by the single particle-level observation are explained. The analysis of the structures reveals their formation mechanisms.

In Chapter III, following the description of the DLVO interaction between colloidal particles, the idea of inducing anisotropy to DLVO interaction by metallodielectric patchy particles is described. Next, our particle fabrication and experimental method are described. Then, we show the results of the selective adsorption of the particles to metal surface. Finally, we describe the formation of the coated structure of metal particles by patchy particles.

In Chapter IV, we summarize the whole study and describe the future perspectives of structure formation using patchy particles.

Chapter II

Elucidation of self-assembled structures in amphiphilic Janus particles-water-oil ternary system

1 Introduction

1.1 Pickering emulsions

When immiscible fluids such as water and oil, and water and air are mixed finely, the respective fluid domains coalesce immediately and the fluids separate macroscopically. When a colloidal particle exhibits partial wetting to the interface between immiscible fluids, it can be stably adsorbed on the interface. The dense colloidal particles adsorbed on the interface prevent the fusion of the interface (cf. Figure 17) and stabilize the dispersion state of immiscible fluids; that is, the fluids are emulsified with the particles [45–48]. Such an emulsion stabilized by solid colloidal particles is called Pickering(-Ramsden) emulsion [49]. Pickering emulsions appear in various materials in nature and industry such as foods and cosmetics, playing characteristic roles in their physical properties and functionalities [50–52]. In general, Pickering emulsions have superior interface stability to conventional emulsion stabilized by surfactant molecules [53, 54].

Here we consider the adsorption of isotropic spherical particles to the interface between immiscible polar liquid (“water”) and apolar liquid (“oil”) (Figure 18). As shown in Figure 18, the area of the water-oil interface decreases by the adsorption of the particle to the interface. When the particle exhibits partial wetting at the water-oil interface, the interfacial energy of the system including the energy at the particle surface decreases by the adsorption of the particle from the water or oil phase. Since the interfacial energy is the product of the interfacial tension and the area, the change of the energy of the system is expressed as

$$\Delta E = E_1 - E_0 = -\pi r^2 \gamma (1 \pm \cos \theta)^2, \quad (1)$$

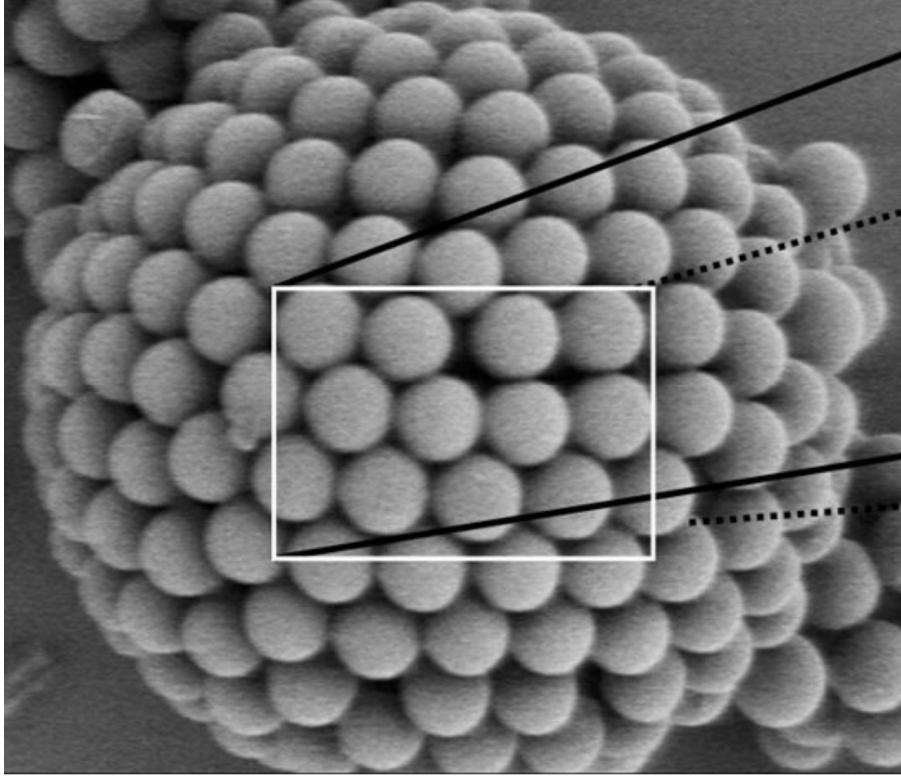


Figure 17. A spherical shell of densely-packed colloidal particles (colloidosome) at an interface [55].

where E_0 and E_1 are the interfacial energy of the system before and after the adsorption of the particle, and r , γ , θ are the radius of the particle, interfacial tension of the water-oil interface, and the contact angle between the particle surface and water-oil interface, respectively. In equation (1), \pm corresponds to the adsorption from the two liquid phases, and usually the one with $1 \pm \cos \theta < 1$ is taken as the adsorption energy of a particle. The decrease of the water-oil interface by a colloid, e.g. a mesoscopic scale particle whose diameter is typically tens of nanometers to micrometers is much larger than that of molecules. Therefore, the adsorption energy of a colloidal particle is much larger than that of molecules. For example, the adsorption energy is $-2750k_B T$, when a spherical particle with a radius of 10 nm are adsorbed on a water-toluene interface ($\gamma = 36$ mN/m) at a contact angle of 90° . k_B and T are the Boltzmann constant and absolute temperature, respectively. Since the adsorption energy is much larger than the thermal energy, the adsorption of particles is thermally

1 INTRODUCTION

irreversible. This huge adsorption energy is the origin of the stability of Pickering emulsions.

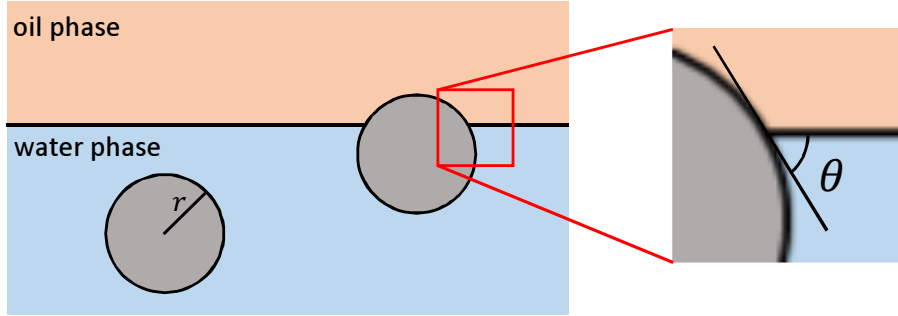


Figure 18. Adsorption of isotropic spherical particle to water-oil interface.

When the oil phase becomes droplets the system is called oil in water (oil/water) type emulsion and *vice versa*. An important point in the formation of Pickering emulsions is that the emulsion type depends not only on the hydrophilicity of the particles and polarities of the solvents but also on the volume ratio of the ternary system and the emulsification process. Majority liquid phase or the liquid phase by to which particles are more wettable tend to be the external, continuous liquid phase of the emulsions generally. Whether the particles are easily wetted by water or oil can be understood from the contact angle between the particle surface and water-oil interface. For example, if the angle between the particle-water interface and water-oil interface is smaller than that between the particle-oil interface and water-oil interface, the particles are more wettable by water. This contact angle θ is determined by the balance of the interfacial tension γ_{sw} at the particle-water interface, the interfacial tension γ_{so} at the particle-oil interface, and the interfacial tension γ at the water-oil interface (Figure 19) described as

$$\gamma_{sw} + \gamma \cos \theta = \gamma_{so}. \quad (2)$$

This is the Young's equation. Figure 20 shows the Pickering emulsion types and the contact angles θ_{ow} (the angle between the solid-water interface and the water-oil interface) in various combinations of solid, water, and oil. The contact angles greatly depend on the combination. The position of a particle at the water-oil interface depends on the contact angle, and the interface covered densely by the particles has

spontaneous curvature when their contact angle is not 90° (Figure 21).

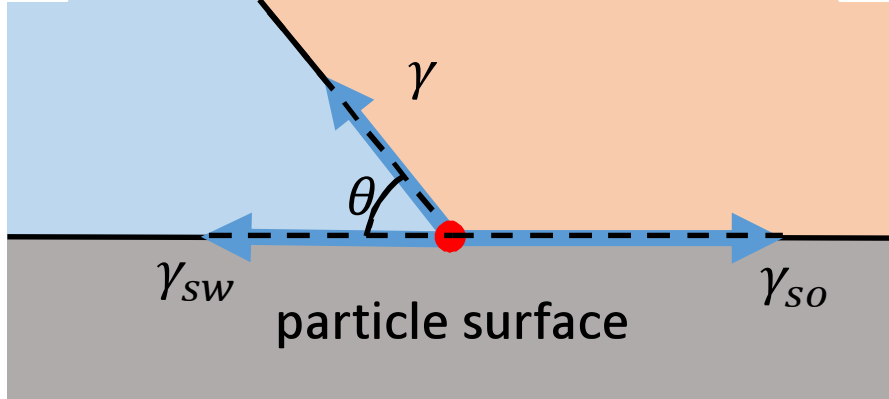


Figure 19. Balance of interfacial tensions at the contact point between water, oil, and particle surfaces.

As described above, since the adsorption energy of particles is much larger than the energy of thermal fluctuation, the free energy of Pickering emulsion systems can be approximated by interfacial energy. When the water-oil interface is covered with solid spherical particles, there is always a gap between the particles (Figure 22), and water-oil interface exists in the gap. The effective tension of the interface densely covered with particles is always positive. The total free energy of a Pickering emulsion is thus minimized when the total area of the particle-adsorbed interface is minimized, that is, when water and oil phase macroscopically separated. This is the thermodynamically most stable, equilibrium state. In general, Pickering emulsions are not at equilibrium but metastable state, and are kinetically stabilized because of the particle layer at the water-oil interface that becomes a steric barrier and prevents coalescence of liquid domains.

Because Pickering emulsions are kinetically stabilized, the formation process of the system also affects the resulting state. Limited coalescence is a typical process of structural development in Pickering emulsions (Figure 23) [57, 58]. The volumes of water, oil, and particles are preserved, and the initial state is that a minority liquid phase is thoroughly divided into a large number of droplets which are sufficiently small and the particles are isolated. Then, the particles are adsorb on the liquid-liquid interface and the droplets repeatedly coalesce and grow in size. Since the droplet

1 INTRODUCTION

Solid	Oil	$\theta_{ow}/^\circ$	Emulsion type
Barium sulfate ^b	Dodecane	0	o/w
	Isopropyl myristate	0	o/w
Calcium carbonate ^b	Dodecane	43	o/w
	Isopropyl myristate	39	o/w
Hydrophilic silica ^a	Dodecane	38	o/w
	Cyclohexane	37	o/w
	PDMS 50 cS	81	o/w
	Isopropyl myristate	32	o/w
	Undecanol	38	o/w
Partially hydrophobic silica ^a	Dodecane	83	o/w
	Cyclohexane	87	o/w
	Isopropyl myristate	101	w/o
	Undecanol	110	w/o
Hydrophobic silica ^a	Dodecane	135	w/o
	Cyclohexane	135	w/o
	PDMS 50 cS	172	w/o
	Isopropyl myristate	> 175	w/o
	Undecanol	151	w/o
Bentonite for organic systems ^b	Dodecane	81	w/o
	Isopropyl myristate	96	w/o
Claytone HY ^b (hydrophobic bentonite)	Dodecane	110	w/o
	Isopropyl myristate	141	w/o
Polystyrene ^a	Dodecane	152	w/o
	PDMS 50 cS	175	w/o
Polytetrafluoroethylene ^a (PTFE)	Dodecane	147	w/o
	Isopropyl myristate	175	w/o
	Undecanol	130	w/o

Figure 20. Contact angle θ_{ow} and emulsion type in various combinations of solid particle, oil, and water [56].

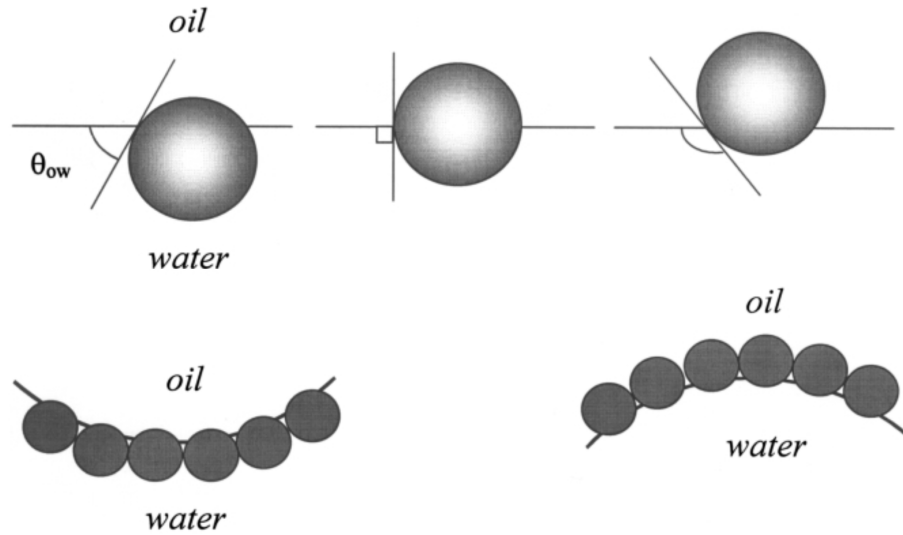


Figure 21. The relation between contact angle θ_{ow} and spontaneous curvature for the interface adsorbing particles densely [56].

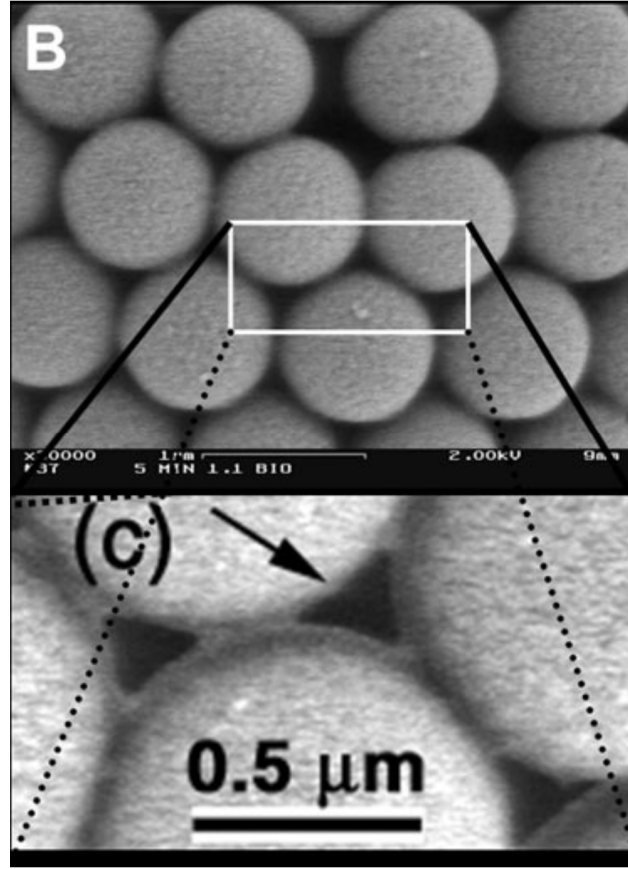


Figure 22. The interstitial gap (arrow) between the densely-packed particles at a droplet surface [55].

surface is not fully covered with the particles at the early stage, they can coalesce by their fusion. The coverage of the particles at a droplet surface increases by the coalescence because the total surface area of the droplets decreases by coalescence whereas the number of the adsorbed particles is preserved. When the surfaces of droplets are densely covered by particles with the progress of coarsening, coarsening halts since the particles are strongly adsorbed on the interface. That is, the system reaches a kinetically stable state.

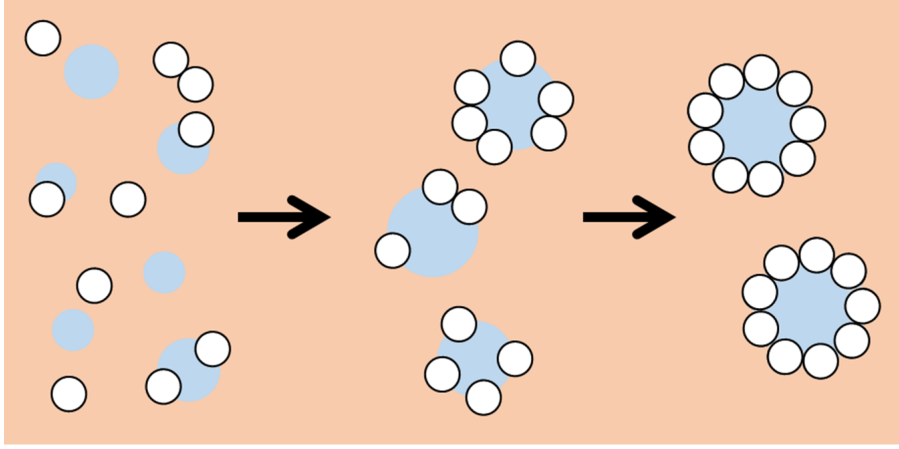


Figure 23. Schematic drawing of limited coalescence process.

1.2 Surface activity of amphiphilic Janus particles and Pickering emulsions with them

Colloidal particles having a hydrophilic and hydrophobic surface exhibit amphiphilicity as known for surface active molecules. When the hydrophilic and hydrophobic surface are both hemispherical, the particle is called amphiphilic Janus particle (AJP) (Figure 24). This particle is the first patchy particle designed and fabricated [59]. This section explains the surface activity and Pickering emulsions of AJPs, and they are compared with the case with isotropic particles.

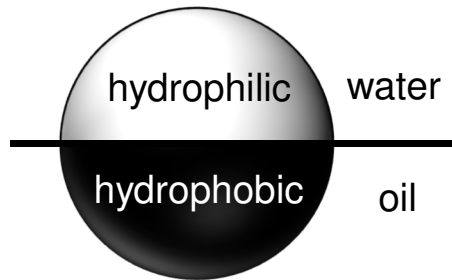


Figure 24. Schematic drawing of amphiphilic Janus particle.

Here we describe the adsorption energy of an AJP (Figure 25). When the hydrophilic/hydrophobic hemispherical surfaces of the amphiphilic Janus particles are

1 INTRODUCTION

completely wetted by water/oil respectively, the change of the interfacial energy by the adsorption of an AJP to water-oil interface is written as

$$\Delta E_{\text{Janus}} \leq -3\pi r^2 \gamma, \quad (3)$$

where r and γ are the radius of the amphiphilic Janus particle and the water-oil interfacial tension, respectively, and ΔE_{Janus} is defined as in equation (1). This equation is derived from the relation between the interfacial energies for complete wetting, $\gamma_{\text{so/sw}} \geq \gamma_{\text{sw/so}} + \gamma$, and $\Delta E = -3\pi r^2 \gamma$ when $\theta = 0^\circ$ or 180° in the Young's equation (2) [60, 61]. Comparing equation (3) with equation (1), the adsorption energy of an AJP can be more than three times as large in magnitude as that of an isotropic spherical particle.

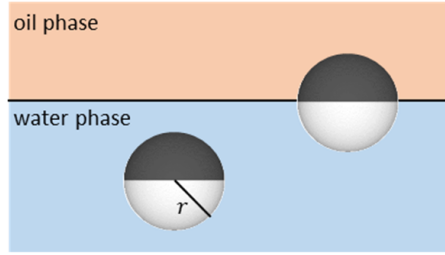


Figure 25. Schematic image of AJPs at water-oil interface and in water phase.

When AJPs are adsorbed on the water-oil interface, if the hydrophilicity and hydrophobicity of each hemisphere are sufficiently high, the three phase contact line is on the hydrophilic-hydrophobic boundary (Figure 26) [62]. At the boundary a range of the contact angle of the water-oil interface is possible, and the arrangement of an adsorbed AJP does not change for some variation in the polarity of the liquid phases (Figure 26).

Next, we consider the stability of Pickering emulsion stabilized by AJPs. When comparing Pickering emulsions by spherical AJPs with those by isotropic spherical particles, the difference in interfacial energy at the particle surface affects the emulsified state, because their shapes are the same. As described, the equilibrium state of the Pickering emulsions with isotropic spherical particles is the macroscopic separation (Sec.1.1 of Chapter II). On the other hand, Aveyard have theoretically shown that, when the amphiphilicity of an AJP is sufficiently large, the free energy of the

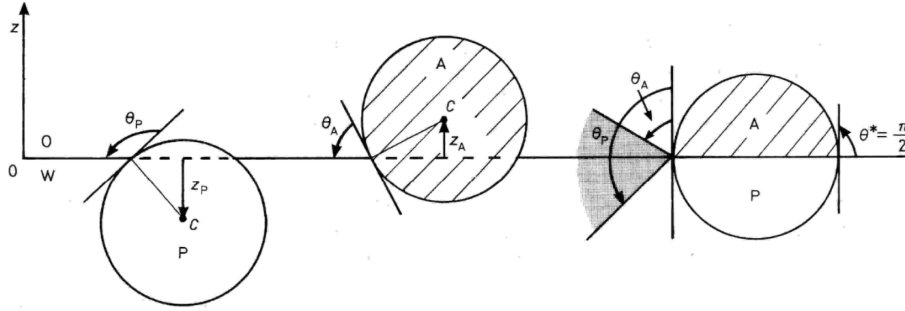


Figure 26. Schematic drawings of AJP (right), hydrophobic particle (center), and hydrophilic particle (left) adsorbed on the interface [62].

Pickering emulsion becomes minimum when all AJPs are adsorbed on the water-oil interface [63]. It indicates Pickering emulsion by AJPs can be thermodynamically most stable (equilibrium state). Because of the high stability of such emulsions, AJP are used in emulsion polymerization or emulsion-based microreactors [64–67].

1.3 Differences and similarities between AJP and amphiphilic molecules

Amphiphilic molecules possess a hydrophilic and hydrophobic group in one molecule (Figure 27). As shown in Figure 27, when amphiphilic molecules are dispersed in a liquid phase, self-assembled structures such as spherical micelles and bilayer membranes appear by hydrophobic/hydrophilic interaction between the molecules. Furthermore, ordered structures composed of these supramolecular unit structures can form. These structures and ordered states depend on the molecular structure such as the size of the hydrophilic head group and the hydrophobic tail. In the amphiphilic molecules-water-oil ternary system, the structures depend also on the composition of the three components.

As described above, AJPs and amphiphilic molecules possess structural similarity. Therefore, the self-assembled structures of AJPs in their dispersions may also strongly depend on the composition of the system and the amphiphilic structure as in amphiphilic molecule systems. It is expected that various aggregate structures and ordered structures can form [34, 68–70]. However, there are also significant differences between AJPs and amphiphilic molecules. Due to the mesoscopic size of the particle, AJPs are adsorbed on the water-oil interface much more strongly than

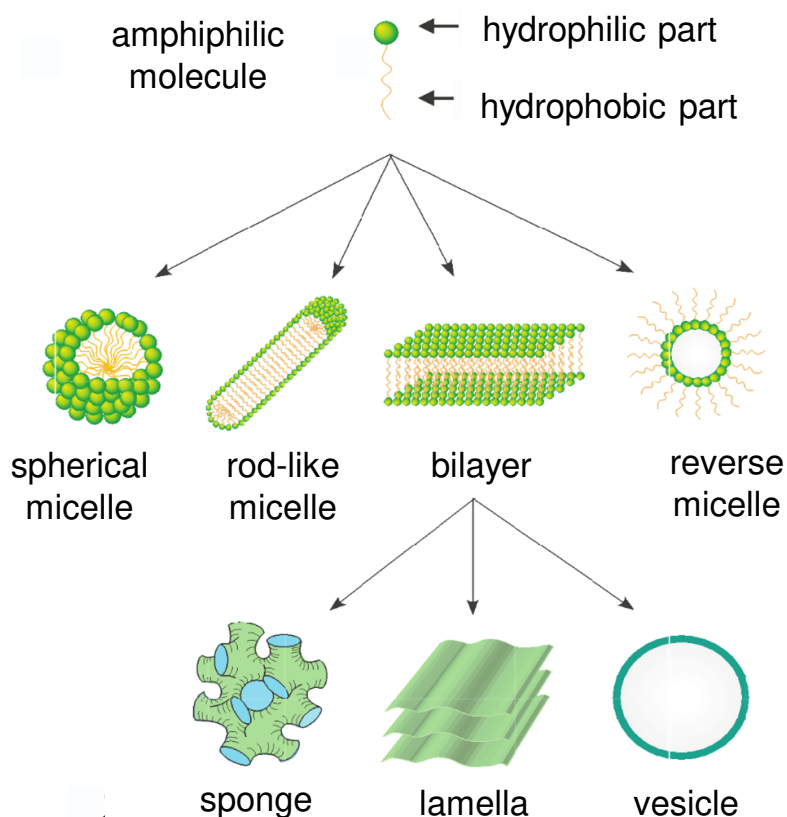


Figure 27. Examples of self-assembled structures by amphiphilic molecules.

amphiphilic molecules, and the adsorption of an AJP is irreversible. In contrast, amphiphilic molecules are at dynamic equilibrium between their adsorption to and desorption from the interface by thermal fluctuations. When AJPs are densely packed in water-oil interface, the hard-body interaction between the particles makes the particle layer solid. In contrast, the molecular layer at the water-oil interface usually exhibits fluidity and becomes a soft membrane. As described above, since small gaps exist between the spherical particles in the adsorbed layer, and water and oil are in contact with each other there, it is possible to exchange substances through the gaps. There are many differences between the colloidal and molecular system, and thus it can also be expected that the AJPs form unique self-assembled structures and/or ordered structures which are different from those of the amphiphilic molecules.

1.4 Motivation and Purpose

As described above, it is expected that AJPs would be superior surfactants to isotropic particles. In addition, AJPs are expected to form self-assembled structures reflecting the amphiphilic structure of the particles, which cannot be formed by isotropic particles. However, most of the experiments with AJP-water-oil ternary systems have focused on the emulsification ability and the stability of the emulsions in macroscopic systems [71–75]. Therefore, the details of the self-assembled structures, their dependence on the experimental conditions, and the structure formation mechanism are still to be clarified.

In order to clarify the whole aspects of the self-assembly in the ternary system, we studied the structures for a wide range of composition of the components by single particle-level observation, and worked on clarifying the structure formation mechanism.

2 Experimental section

2.1 Prepareing AJPs

We prepared AJPs composed of hydrophilic and hydrophobic hemispheres by coating a hemisphere of spherical silica particles with Au and modifying the surface of the Au layer with 1-octadecanethiol (90.0 %, Wako) to make the surface hydrophobic. First, a monolayer of monodisperse silica particles (Hyprecica, UEXC), diameter $d = 3.01 \mu\text{m}$ with size dispersion $\sim 1.5 \%$ coefficient of variation, was prepared at an air-water interface and transferred onto a hydrophilized glass slide [76]. A 50-nm-thick gold layer was thermally deposited onto the monolayer, following a 3-nm-thick chromium layer. This gold layer formed a hemispherical gold cap on the particle [73]. To render the gold surface hydrophobic, the particles were soaked in a 2 mM ethanol solution of 1-octadecanethiol for 24 h. We rinsed the particles (volume $\simeq 10 \mu\text{L}$) three times by dispersing them in 50 mL of ethanol and collecting them with a centrifuge. These particles possessed high amphiphilicity. They show clear amphiphilic Janus nature not only at pure water (18.2 M Ω , Millipore)–*n*-dodecane (99.0 %, Wako) interface (Figure 28) used in subsequent experiments, but also at an interface where

2 EXPERIMENTAL SECTION

the difference in polarity was smaller than that of water-*n*-dodecane. The interface was formed in the mixture composed with ethanol (99.5 %, Wako), dodecane, and a small quantity of pure water. The volume ratio of ethanol and dodecane was 25:75 and the water content was less than 1 % of the total volume. Because of the small water content, this mixture phase separated into ethanol- and dodecane-rich phases at room temperature, roughly at the volume fractions of the ethanol and dodecane content. In Figure 29, AJP can be seen attached to the interface between the two liquid phases, with their hydrophobic Au hemisphere immersed in the dodecane-rich phase and their silica hydrophilic hemisphere in the ethanol-rich phase. Thus, the fabricated AJP had a clear Janus nature with high amphiphilicity.

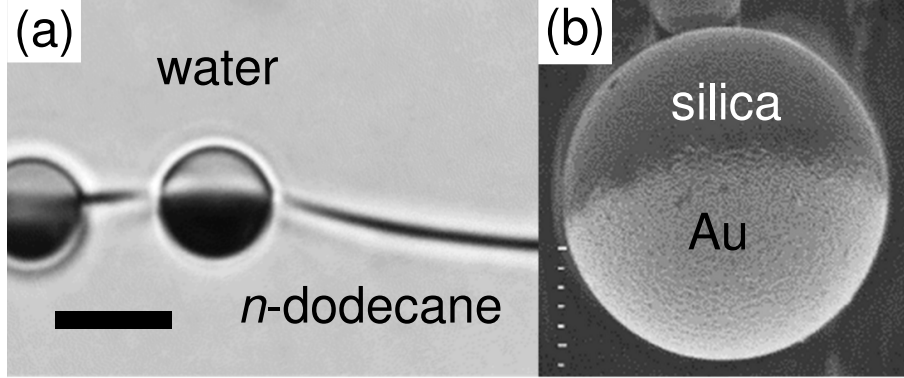


Figure 28. Amphiphilic Janus particles attaching to a liquid-liquid interface. (a) Au optical microscope image of AJP at a water-dodecane interface. The black and white regions of a particle are, respectively, the hydrophobic part (Au-coated surface) and hydrophilic part (silica surface). The scale bar is $5.5 \mu\text{m}$. (b) A scanning electron microscope image of a spherical silica particle with a hemisphere coated with Au. The white and gray regions of the particle are, respectively, the Au-coated surface and the silica surface. The radius of the particle was $2.6 \mu\text{m}$ for visual clarity.

2.2 Structure formation and observation

We prepared a ternary system comprising AJP, pure water, and *n*-dodecane. We used a volume ratio of water to the particles, $\alpha = V_W / V_p$, over the range $0.00 - 8.28$, where both V_W and V_p were precisely measured and were up to a few microliters. The volume of dodecane was $100 - 200 \mu\text{L}$. The water was thus the minority liquid phase

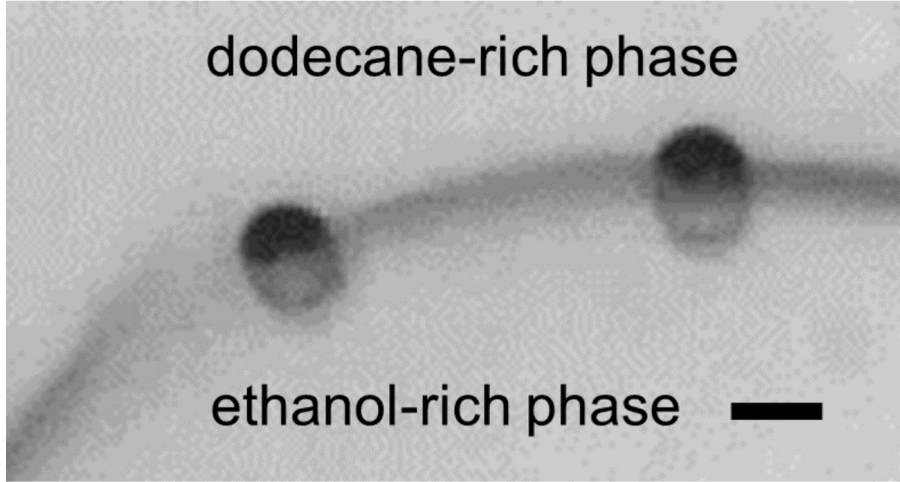


Figure 29. An optical microscope image of amphiphilic Janus particles attached to the interface between dodecane-rich and ethanol-rich phases. The black and white regions of a particle are, respectively, the hydrophobic part (Au-coated surface) and the hydrophilic part (silica surface). The scale bar is 5 μm .

in all samples so that the water domain was isolated and enclosed by the particles. For each sample preparation, the amount of AJP was weighed and the value was converted to volume with the mass densities of the particle and gold. The AJPs were dispersed in dodecane in a polypropylene tube with an ultrasound bath (38 kHz, 100 W)(US-102, SND Inc.) for ~ 5 min. Next, when $V_W \geq 0.5 \mu\text{L}$, the required amount of water was added to the AJP-dispersed dodecane with a micropipette, followed by the ultrasonic mixing for ~ 60 s. When $V_W < 0.5 \mu\text{L}$, a larger amount of water was first dispersed in dodecane homogeneously by ultrasonication, and then the calculated amount of the water-dispersed dodecane containing the required V_W was added to AJP-dispersed dodecane, followed by ultrasonic mixing for ~ 60 s. This process enables precise control of V_W and through break-up of such a tiny amount of water (cf. Figure 30). After the self-assembled structure formation in a sample under gentle stirring by hand, some amount of the sample, $\sim 20 \mu\text{L}$, was taken and diluted in dodecane $\sim 100 \mu\text{L}$ to isolate each cluster/emulsion droplet. This diluted sample was observed with optical microscopy: BX50 (Olympus) with objective lenses Plan 40x/0.65 and Ach 20x/0.40, and TE2000-U (Nikon) with objective lenses PlanApo VC 100x/1.40, PlanApo VC 60x/1.40, PlanFluor 40x/0.75 Ph2 DLL and PlanFluor

3 RESULTS AND DISCUSSION

20x/0.50 Ph1 DLL, dependent on the required magnification. No noticeable effect of the dilution process on their structures was observed under the microscopy. We prepared the samples with different α to investigate the dependence of self-assembled structures on it.

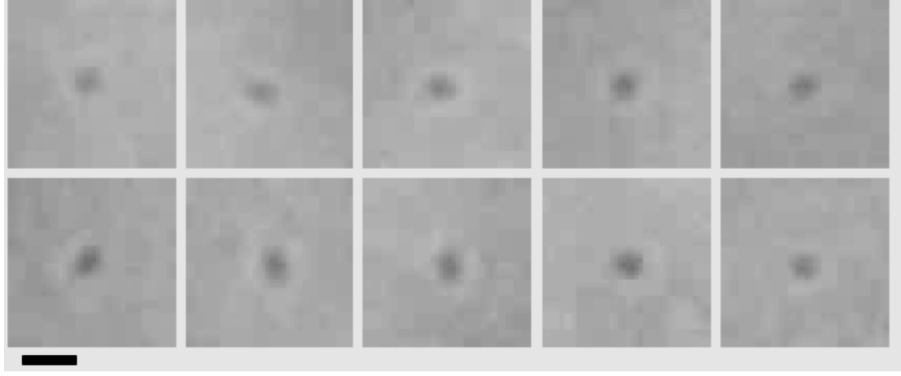


Figure 30. Optical microscopy images of water droplets wetting a glass coverslip in dodecane. Apparently, the diameter of the wetting droplets is $\lesssim 1 \mu\text{m}$: When the diameter is $1 \mu\text{m}$, the corresponding diameter of the floating droplet is $0.52 \mu\text{m}$. It follows that the diameter of water droplets after the agitation should have been less than $1 \mu\text{m}$ typically. The scale bar is $1 \mu\text{m}$.

3 Results and Discussion

3.1 The aggregates and the change in structure

This section first qualitatively describes the change in structure of the ternary system with increasing water content, α . With increasing α , (inverse) small, micelle-like clusters appeared, followed by anisotropic growth into rod-like shapes, and finally spherical emulsion droplets were formed (Figure 31 (b-k)). At $\alpha = 0.00$, random aggregates simply were formed by the van der Waals attraction between the particles (Figure 31 (a)). The attraction between bare silica particles is strong enough to irreversibly aggregate in dodecane, explaining why there was no selectivity for bonding surfaces observed, although a stronger attraction was expected between Au surfaces than between Au and silica or between silica surfaces due to the large Hamaker constant of Au. Adding a small amount of water ($\alpha = 0.09$) caused small clusters in which

3 RESULTS AND DISCUSSION

hydrophilic surfaces were bonded to one another with an inverse micelle-like internal structure (Figure 31 (b)). The micelle-like clusters coexisted with random aggregates. Larger micelle-like clusters were observed with an increase in α . Simultaneously, the number ratio of the micelle-like clusters to random aggregates increased with α , and random aggregates were not observed for $\alpha > 0.27$. When the sizes of small clusters exceeded about 15 particles, the clusters exhibited unidirectional anisotropy in shape. The clusters with clear rod-like shapes appeared at $\alpha \geq 0.16$ (Figure 31 (c-e)). With further increases in α , almost all clusters became rod-like and their widths slightly increased, as shown in Figure 31 (c-e). For $\alpha \geq 0.39$, spherical emulsion droplets (colloidosomes) with a water inner phase appeared. In Figure 31 (j), AJP can be seen attached to the water-oil interface, reflecting their amphiphilic Janus structure and forming a monolayer. With an increase in α , the size of the spherical emulsion droplets and the number ratio of them to all aggregates increased. For $\alpha \geq 0.66$, finally, the system formed an emulsion, in which almost all structures were spherical droplets (Figure 31 (g-j)). A diagram of the α -ranges for each of the characteristic structures is shown in Figure 31 (k). At the intermediate concentration where rod-like micelles and spherical droplets coexisted, a structure was observed with a thickness that differed somewhat from other parts (Figure 31 (f)). This may have been an intermediate structure between rod-like and spherical droplets. The reason for the increase in thickness of the rod-like clusters observed in Figure 31 (c-e) is not only that more particles are attached to the cluster to eliminate hydrophilic surfaces exposed to the external environment, which is apparent by comparing Figure 31 (c) and (d), but also that the rods slightly swelled because of the inner water phase. However, the inner structure of micelle-like clusters has not been observed in detail at this stage. The way in which thickness changed in Figure 31 (f) and the existence of swelling remain uncertain.

There is a similarity between the observed structural changes induced by increasing the water content for the AJP and those known for surfactant molecules. At low water content, the formed clusters were similar to the spherical and rod-like micelles that occur in a binary system of surfactant and solvent. At $\alpha \gtrsim 1$, where clusters can swell, emulsions composed of spherical droplets appeared, which are well-known in (micro)-emulsions of surfactant systems. However, the particles showed no thermal motion in the clusters and emulsion droplets, indicating much larger interparticle and

3 RESULTS AND DISCUSSION

particle-interface interaction compared with thermal agitation. Thus, the structures with AJP did not relax thermally; that is, they are trapped deeply within metastable states, which differs from the dynamic equilibrium structures found in surfactant systems including micro-emulsions. Such a metastability has often been observed in mesoscopic particle systems, such as in Pickering Emulsions formed with homogeneous particles [45]. We therefore consider that the continuous change in the ratio of respective structures with the increase of α was predominantly caused by stochastic and/or kinetic formation of metastable structures and cannot be related directly to the transition between equilibrium states. It would be noteworthy that the emulsion droplets can be regarded as swollen spherical micelles of a micro-emulsion when the emulsion with AJP is (almost) at equilibrium, though it would not be the case here as discussed later.

3.2 Detail of micelle-like cluster and the formation mechanism

In this section, the formation mechanism of micelle-like clusters observed at low water content is discussed. From the microscopic observation of randomly sampled small clusters composed of two or three particles for $\alpha \leq 0.27$ (Figure 32 (a)), the ratio of bonds that were not formed between hydrophilic surfaces is large at $\alpha = 0.09$, whereas most bonds were formed between hydrophilic surfaces at $\alpha = 0.27$. Figure 32 (b) shows the orientation of hydrophobic surfaces in typical clusters over the α -range. With an increase in α , the hydrophobic surfaces of the particles tended to face outwards from the cluster, i.e. forming inverse micelle-like structures enclosing the hydrophilic surfaces, as observed in Figure 31. In inverse micelles formed with surfactant molecules in apolar solvents, the condensation force arises from the attraction between the hydrophilic parts of the molecules (or the repulsion between hydrophilic parts and apolar solvents, or hydrophobic parts). For AJP in a polar solvent, the formation of micelle-like clusters through attraction between hydrophobic surfaces has been also reported [11, 32]. However, because the bonds between hydrophilic surfaces increased with α in this study (Figure 32 (a)), the formation of clusters cannot be explained simply by the attraction between hydrophilic surfaces in an apolar solvent. The results can be decently explained with the selective attraction between hydrophilic surfaces induced by water rather than hydrophilic-hydrophilic attraction.

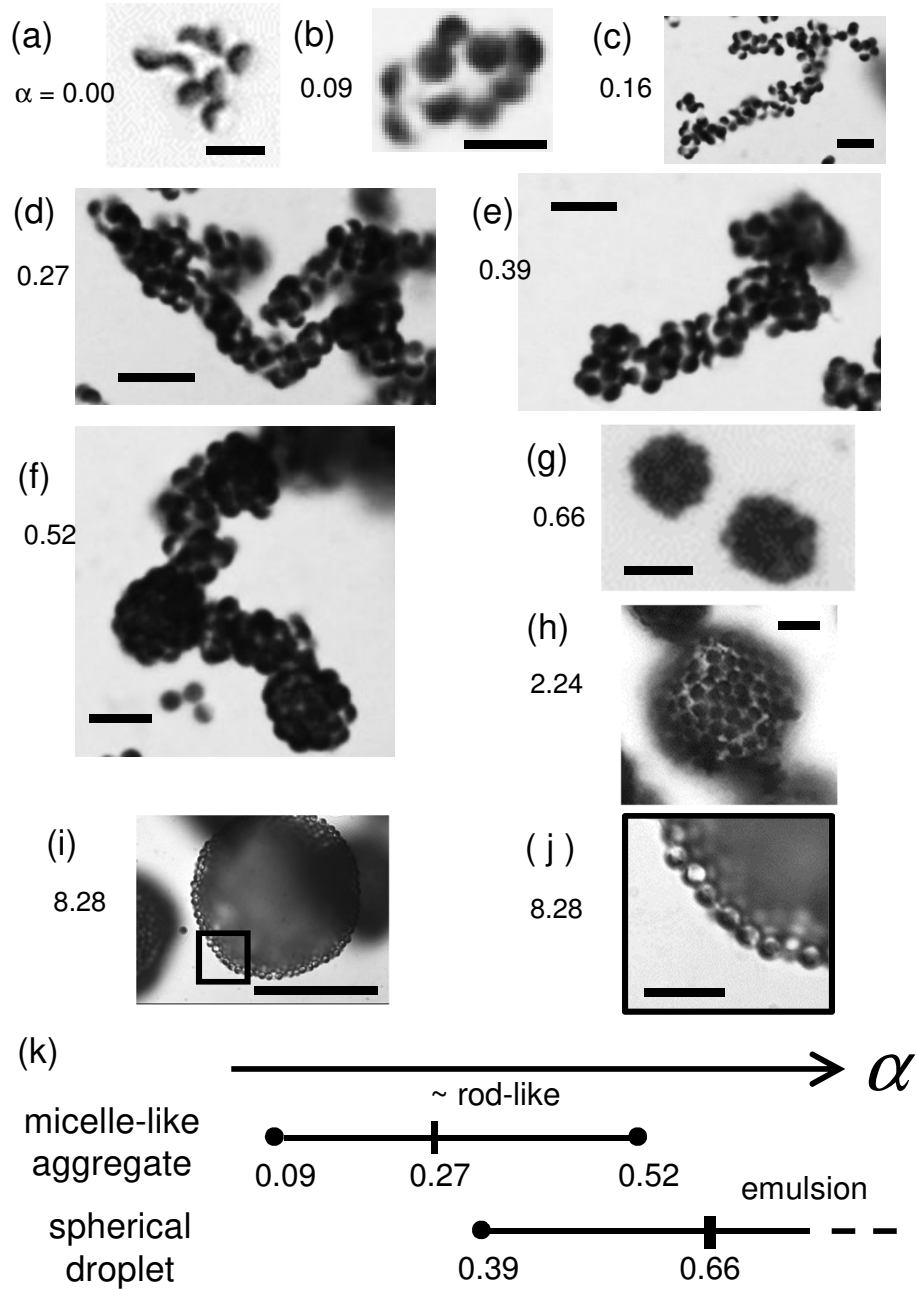


Figure 31. α -dependence of the morphology in self-assembled structures. (a-i) Optical microscope images of typical structures formed at respective α . (a) Random aggregate. (b) Small micelle-like cluster. (c-e) Rod-shaped micelle-like clusters. (f) Structure observed at a value of α where rod-shaped micelle-like clusters and spherical droplets coexist. (g-i) Spherical droplets in emulsions. (i) Hemispherical droplet attached to the bottom of the observation cell. (j) Magnified image of the framed region in (i). (k) Diagram of the α -range of the observed structures. The scale bars are $5 \mu\text{m}$ in (a) and (b), $10 \mu\text{m}$ in (c)-(h) and (j), and $50 \mu\text{m}$ in (i).

3 RESULTS AND DISCUSSION

We speculate that this attractive force acts through a capillary bridge of a water droplet between hydrophilic surfaces as shown in Figure 32 (c). In the mixture of homogenous particles and two immiscible liquids, it is known that the minority liquid phase that is wetted by the particles “glues” them together by the strong attraction between them [77–80]. The capillary force is typically much stronger than other interparticle interactions such as van der Waals and electrostatic force in colloidal systems [77, 78]. The force is calculated as $F = 2\pi r_1 \gamma + \pi r_1^2 \Delta P$, where r_1 is the neck radius of a capillary bridge and ΔP is the Laplace pressure. (Figure 33) When a capillary bridge is very small, its shape is approximated as in Figure 33 (a) for $r_1 \gg r_2$. The force asymptotically approaches its maximum, $F_{max} = 2\pi a \gamma \cos \theta$, where a is the radius of the particles, with the decrease in the bridge size, where the Laplace pressure is dominant. The force decreases with the increase in the capillary bridge size. For a large cylindrical liquid bridge as shown in Figure 33 (b), e.g. $F = \pi a \gamma \cos \theta$; that is, the size dependence of the force is not significant compared with the differences between the capillary force and other typical inter-particle forces as shown in Ref. [77]. In our system, the capillary force between two silica surfaces in contact is described as $F_c = 2\pi a \gamma \cos \theta \approx 400$ nN, where the surface tension between water and *n*-dodecane at room temperature $\gamma = 53$ mN/m [81] and the contact angle of water in dodecane on a silica surface $\theta \approx 40^\circ$ [56]. The typical value for the van der Waals force is described as $F_{vdW} = Aa/12s^2 \approx 1$ nN, where the typical interparticle distance $s = 1$ nm is given by assuming the surface roughness is 1 nm and Hamaker constant $A \approx 10^{-20}$ J for silica particles in water. The force between gold hemispheres is described as $F_{vdW}^{gold} = Aa/12s^2 \approx 50$ nN, where $A \approx 40 \times 10^{-20}$ J. Thus, the capillary force must be generally much larger than the van der Waals forces in our system because the former does not significantly depend on the droplet volume.

During the structure formation process, water was initially broken into small-diameter droplets $\lesssim 1 \mu\text{m}$. Water partially wets the silica surface in *n*-dodecane, thus the droplets would cover a relatively small area of the hydrophilic silica surface at a low water content (e.g. $\alpha = 0.09$, see the left image in Figure 32 (d)). The number of possible capillary bridges between hydrophilic surfaces is therefore relatively small under such conditions, resulting in a low ratio of hydrophilic-hydrophilic bonding. With increasing water content, a larger area on the hydrophilic surface can be covered with water droplets (the right image in Figure 32 (d)), and hydrophilic-hydrophilic bonding

3 RESULTS AND DISCUSSION

becomes predominant. In addition, experimental [11,32] and theoretical [82] studies have reported that a rod-like structure is most stable when a hemisphere of Janus particles aggregates through a short-range attraction. This explains the formation of the rod-shaped micelle-like clusters when hydrophilic-hydrophilic bonding becomes predominant with increasing α .

3.3 Detail of spherical droplet and the formation mechanism

This section discuss the structure of emulsion droplets formed at high water content. The size of the droplets apparently increases with water content (Figure 34 (a)). For $\alpha > 0.66$, where almost all of the structures in the system were spherical droplets, their standard deviation and average radius \bar{r} (Figure 34 (b)), and the distribution of their radii (Figure 34 (c)) were obtained by image analysis. The definition of r is given in the schematic image shown in Figure 34 (b). The microscope images of the droplets shown in Figure 34 (a) include the particles attached to the interface and thus the observed radius r^* is given as $r^* = r + a$. \bar{r} was almost proportional to α , as shown in Figure 35 (b). The size distribution was narrow at all values of α , 0.66 - 8.28 as shown in Figure 34 (b) and (c). The average of coefficient of variation over the α -range was 24 %.

The linear relationship between \bar{r} and α , i.e. $\bar{r} \propto V_W$ and $\bar{r} \propto V_p^{-1}$, appears to have arisen from the limited coalescence upon Pickering Emulsion formation [57] as follows. It is assumed that the minority liquid phase was initially fully broken into tiny droplets, and all particles became attached irreversibly to the liquid-liquid interface during the coalescence process. The droplets then coalesced to each other until the layer of attached particles became sufficiently dense to kinetically prevent their fusion. Thus, the total surface area of droplets coincided with the liquid-liquid interfacial area that particles could possibly cover by forming the dense layer of attached particles, resulting in the proportionality mentioned above. The surface area density of droplets $S(r)$ followed the log-normal distribution (see the inset in Figure 34 (c)), which also appears in the case of limited coalescence [57, 58]: $S(r) \propto \frac{1}{\sqrt{2\pi}\sigma r} e^{-(\ln(r-M))^2/2\sigma^2}$, where M and σ are the parameters whose combinations are related to the mean and variance of the distribution.

We compare our experimental results with the following model, which is based on

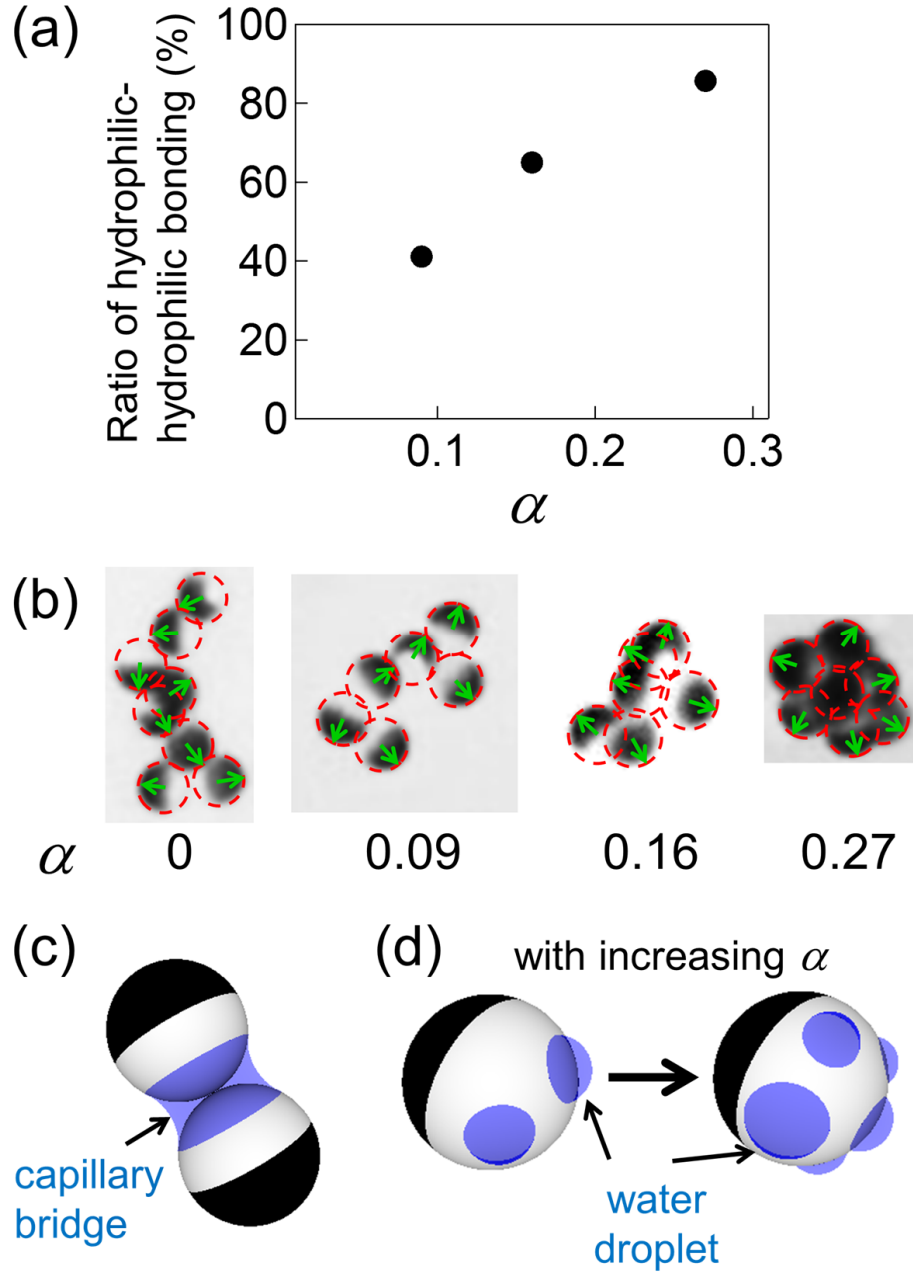


Figure 32. Bonding between AJP in micelle-like clusters. (a) Ratio of bonds between hydrophilic hemispheres (silica surfaces) to the total bonds in small clusters. The number of analyzed particles were 30, 28 and 19, respectively, for $\alpha = 0.09, 0.16$, and 0.27 . (b) Orientation of the hydrophilic surfaces. The broken lines represent the outlines of the particles. The arrow indicates the direction of the center of a hydrophobic hemisphere in two-dimensions. (c) Schematic of Janus particles bonded by a capillary bridge between their hydrophilic surfaces. (d) Schematic of particles wetted by water droplets on their hydrophilic surfaces.

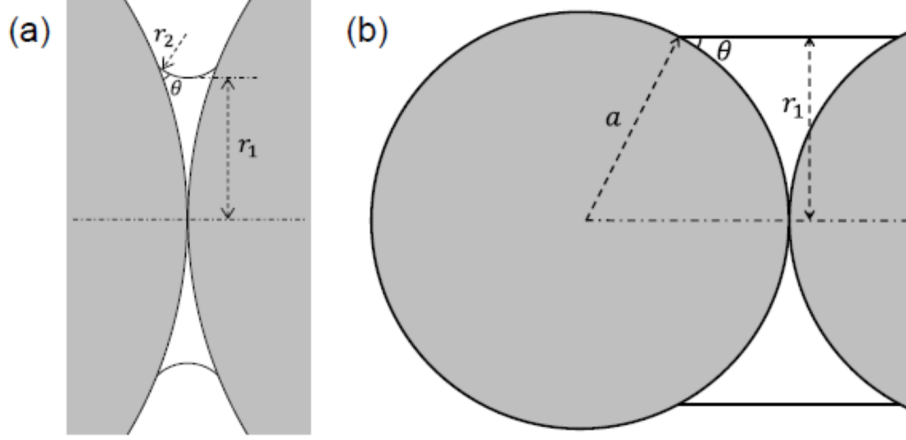


Figure 33. Schematics of a capillary bridge between particles at contact. (a) A small capillary bridge, where $r_1 \gg r_2$. (b) A cylindrical bridge, where $r_1 = a \cos \theta$.

limited coalescence and takes into account the volume of the attached particles (the inset in Figure 34 (b)). We assume that (i) droplets are monodisperse ($\bar{r} = r$ in this model), (ii) the influence of curvature of the droplets can be ignored, (iii) the boundary between hydrophilic and hydrophobic surfaces of AJP lies at the water-dodecane interface, and (iv) the interfacial coverage of AJP, C , which is defined as the ratio of the area covered by particles to the lateral surface area of a droplet, $4\pi r^2$, is constant. The resultant relation between r and α is therefore

$$r = 4aC\alpha + 2aC \quad (4)$$

where $a = 1.5 \mu\text{m}$. For this calculation, we used the surface area and volume of the spherical body shown by the dashed circular line in the inset of Figure 34 (b), thus half of each attached particle is included in the body. The total surface area of the spherical body S_d is

$$S_d = 4\pi r^2 n_d \quad (5)$$

where n_d is the number of droplets and $\bar{r} = r$ here. In limited coalescence, all the particles attach to the surface to give coverage C . Thus, CS_d gives the total cross-sectional area of the particles at the surface expressed as

$$CS_d = \pi a^2 n_p = \frac{3V_p}{4a} \quad (6)$$

where $n_p = V_p/v_p$ is the number of AJPs; V_p is the total volume of AJPs and $v_p =$

3 RESULTS AND DISCUSSION

$4\pi a^3/3$ is the volume of one AJP. The total volume of the spherical body V_d is

$$V_d = \frac{4}{3}\pi r^3 n_d = V_W + \frac{1}{2}V_p \quad (7)$$

where V_W is the total volume of water. Using $V_d = rS_d/3$, equations (6) and (7) give

$$\frac{V_p}{4aC}r = V_W + \frac{1}{2}V_p, \quad (8)$$

leading to equation (4). The experimental result of \bar{r} can be fitted well by equation (4) using $C_{fit} = 0.60$ as a fitting parameter (Figure 35 (b)). Together with the log-normal distribution of $S(r)$, the emulsification in our experiment can be explained well by limited coalescence. A requirement for the process, strong agitation for mixing, was observed in practice, as mentioned in the experimental methods section.

The value of C_{fit} obtained is smaller than that for the close-packing of spheres, $C_{cp} = 0.91$. The interfacial coverages obtained directly by microscopy observation of the droplets surface, C_{exp} , were 0.61 - 0.71 for $\alpha = 4.14 - 7.44$ (Figure 35 (a)), respectively. The reason that C_{fit} and C_{exp} are smaller than C_{cp} is probably that the anisotropic interaction between particles originated from a deformation of the liquid-liquid interface. There are small undulations of the boundary between hydrophilic and hydrophobic surfaces on an amphiphilic Janus particle (Figure 28 (b)). The undulations deform the interface in the vicinity of the attached particle and induce anisotropic interaction between the particles [83]. This interaction is also referred to as capillary interaction; however, the geometry of particles was different from that for capillary bridges described above. In Ref. [83], Park et al. reported the formation of a loosely packed layer of AJP at a water-oil interface in a similar system. This anisotropic interaction would hinder the closest packing of AJP on the droplet surfaces. In addition, the slightly smaller values of C_{fit} than C_{exp} was caused by the size distribution of droplets (Figure 34 (c)). Considering the size distribution, the total surface area of droplets was estimated for $\alpha = 4.14 - 7.44$ by approximating the experimentally obtained surface area density to a log-normal distribution (cf. the inset in Figure 34 (c)). These re-calculated total surface areas for respective α are smaller by 5 % on average than those estimated by assuming a constant radius, \bar{r} , for the same total volume of droplets. The corrected values of C_{fit} with the re-calculated total surface areas, C_{fit}^{disp} , approach C_{exp} and agree within statistical errors (Figure 35 (a)).

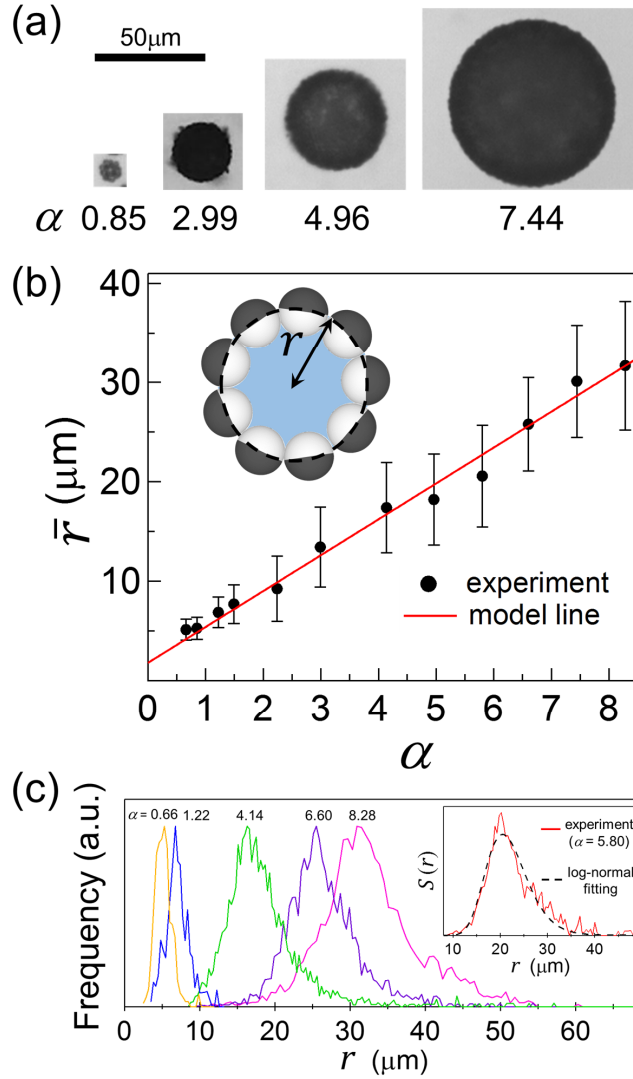


Figure 34. Dependence of emulsion droplet size on α . (a) Typical optical microscope images of spherical droplets formed at $\alpha = 0.85, 2.99, 4.96$, and 7.44 . (b) Dependence of average radius of droplets \bar{r} on α . The error bars represent their standard deviations. The solid line is the best-fit by equation (4). Inset is a schematic of a cross-sectional view of a spherical droplet. The radius of the droplet r is measured from its center to the liquid-liquid interface, which is at the middle of the attached particles. (c) Distribution of the radius of droplets at various α . The plots are normalized by their peak heights. Inset is the distribution plotted as a surface area ratio, i.e., surface area density, at $\alpha = 5.80$. The broken line is the best-fit to a log-normal distribution.

3 RESULTS AND DISCUSSION

The linear relationship observed between r and α in Figure 34 (b) simply indicates that the total surface area of droplets was proportional to the total number of particles, and there was no direct relationship between the area and the number of the particles that actually attach to the droplet surfaces. Hence, we estimated the total volume of the attached AJPs at respective α in the experiment from the surface coverage C_{exp} , the distribution of droplet radius obtained by observation (Figure 34 (c)), and the volume of the water added to the sample. These values estimated from experimental results show good agreement with those of the particles added during sample preparation (Figure 35 (b)). This agreement indicates that almost all particles directly contributed to the stabilization of the droplets.

Emulsions are formed even at fairly low values of α , especially $\alpha < 1$, where the volume of water is smaller than that of the particles, as described above. This result also indicates the high surface activity of the AJP. However, the influence of the curvature of a droplet cannot be negligible at this region of α [84], and it is necessary to explicitly consider the arrangement of the individual particles and shape of the liquid-liquid interface. Elucidating the mechanism behind the formation of emulsions for a small quantity of the minority liquid phase, including the transition from rod-like clusters to spherical droplets, is left for future studies.

In the above discussion, we quantitatively showed that AJPs exhibit excellent surface activities to stabilize droplets where all the particles contribute to the stabilization after the limited coalescence process. Although these features are known for Pickering emulsions of homogenous particles, AJPs possess advantages, as described in the Introduction. The elucidation of AJP emulsification from the lower limit of the minority liquid phase ratio in this study would therefore contribute to their application. The agreement of the emulsion state with the limited coalescence model shown e.g. by the log-normal distribution in Figure 34 (c) suggests that the droplets are kinetically stabilized in this experiment and thus they do not correspond to swollen micelles of a microemulsion. The equilibrium emulsion state is also difficult to achieve by such a low interfacial coverage of particles at the droplet surface. In addition, because a spherical droplet (colloidosome) has interstitial space between the particles even at the closest surface packing state ($C_{cp} = 0.91$), the structure is applicable to permeable microcapsules. Our results suggest the possibility of controlling the surface coverage of the colloidosome, i.e. control of porosity using the undulation of

3 RESULTS AND DISCUSSION

the boundary between hydrophilic and hydrophobic surfaces of an amphiphilic Janus particle, which would also be useful for controlling permeability.

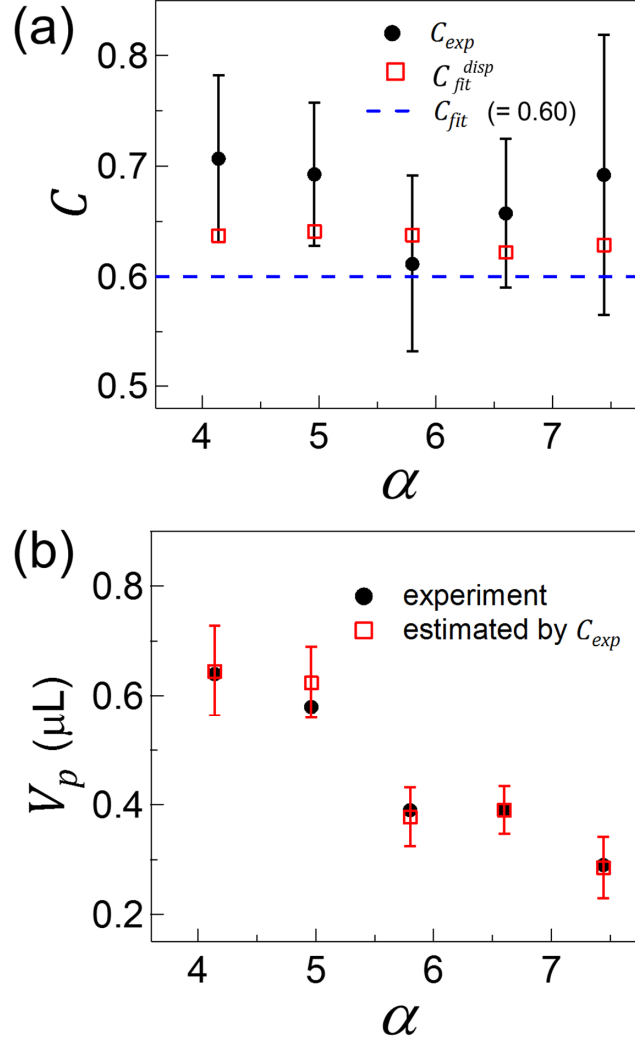


Figure 35. Coverage of AJP on emulsion droplets. (a) Surface coverage of AJP obtained from microscopic observation, C_{exp} , from fitting equation (4), C_{fit} , and the corrected values considering droplet size distribution, C_{fit}^{disp} . The numbers of analyzed droplets for the C_{exp} data corresponding to $\alpha = 4.14, 4.96, 5.80, 6.60$, and 7.44 are, respectively, 13, 14, 16, 14, and 8. (b) Comparison between the amounts of AJP attached to the droplet surface estimated from microscopic observation and those in a sample, i.e., the amounts added during sample preparation. In this range of α , V_p monotonously decreases because we increased α by decreasing the volume of particles V_p .

4 Summary and conclusion

In this study, we observed the internal structures in a ternary system composed of amphiphilic Janus particles comprising hydrophilic and hydrophobic hemispheres, water and oil by varying the ratio of the minority liquid phase (water) to the particles over 2 orders of magnitude. With increasing water content, the self-assembled structures showed a transition from micelle-like clusters formed by anisotropic interaction between AJP to emulsions where spherical droplets were stabilized by the surface activity of AJP. At low water content, the strong attraction due to capillary interactions induced by tiny water droplets selectively appeared between the hydrophilic hemispheres, forming (inverse) micelle-like clusters. When the clusters were large, the shape of the structures became rodlike, reflecting the Janus structure of the particle where the sticky surface is hemispherical. When the water content was large enough to fill the interstices between hydrophilic surfaces, i.e. the volumes of AJP and water became equivalent, droplets covered with AJP (colloidosome) were formed.

This is the first experimental study that systematically elucidates the remarkable change in self-assembled structures in the ternary system of AJP-water-oil through changes in composition. We have demonstrated that the chemical duality, i.e. amphiphilicity, of mesoscopic particles induces self-assembly which is qualitatively the same as that in microemulsions of surfactant molecules. On the other hand, there is an essential difference due to the size of surfactant: The mesoscopic size of AJP makes the interparticle and particle-interface interaction much larger than thermal agitation. The self-assembly in AJP system is therefore irreversible and the structures are kinetically, not thermodynamically, stabilized, being different from dynamic equilibrium structures in microemulsions. In addition, our study clearly shows agreement between experiment and a simple theoretical model for the dependence of emulsion droplet size on the composition of the system. The latter has previously been studied experimentally for homogeneous particles [57] but only theoretically for nonspherical AJP [58].

Our experimental results clearly show that AJPs have the characteristics of both surfactant molecules and homogeneous colloids as emulsifiers. The formation of micelle-like clusters is useful to homogeneously disperse the particles while avoiding

4 SUMMARY AND CONCLUSION

large agglomerate formation, as a preliminary step for emulsification. The emulsification of AJP is explained by limited coalescence, as in the case for homogeneous particles. This study provides fundamental understanding of the use of AJP as a superior emulsifier compared with homogeneous particles. The elucidation of the basic mechanism behind structure formation of AJP is also expected to be useful in understanding emulsification by anisotropic biomolecules such as proteins.

ChapterIII

Control of adsorption behavior of metal-patchy dielectric particles utilizing anisotropy in DLVO interaction

1 Introduction

1.1 DLVO interaction

As described in Sec.4 of Chapter I, the DLVO theory describes the interaction that works between colloidal particles in solution as the sum of van der Waals (vdW) attraction and the repulsion by the electric double layer (EDL). DLVO interaction is the most fundamental and widely employed interaction in discussing the dispersion stability of colloidal particles. vdW interaction is universal between materials. In a polar solvent such as water, the surface of a colloidal particle often has a surface charge, and thus EDLs are formed, inducing the EDL repulsion between the colloidal particles.

1.1.1 vdW interaction

vdW interaction is a kind of electrostatic interaction depending on the dielectric constant and its frequency dependence, the polarization of molecules, etc. In addition to the properties of the materials, the morphology and thickness of the interacting objects affect the interaction. In this section, the dependence of the interaction on these parameters is explained using the theoretical equation of non-retarded vdW interaction. When the solid material 1 and material 2 have flat surfaces in parallel separated by the medium 3 (Figure 36), the vdW force between the solid material 1 and 2 per unit area is expressed as follows.

$$f_{\text{vdW}}(D) = -\frac{A_{132}}{6\pi D^3}, \quad (9)$$

where A_{132} is the Hamaker constant when the medium 3 exists between the material 1 and material 2, and D is the distance between the flat surfaces [18].

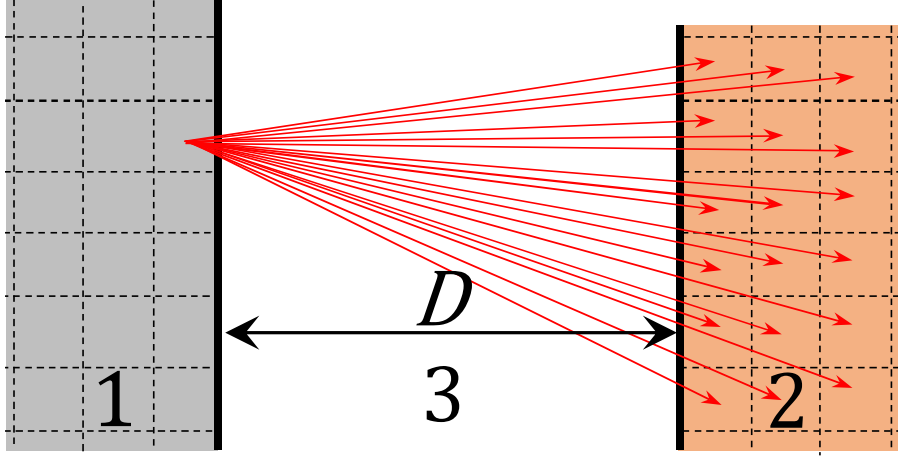


Figure 36. The interaction working between materials 1 and 2.

When the shape of the interacting objects is different, the distance between the micro regions changes from the case in Figure 36. The equations of the vdW interaction between spherical object 1 and flat object 2 (Figure 37) and between spherical objects 1 and 2 (Figure 38) with medium 3 are expressed as follows.

$$F_{\text{vdW}}(D) = -\frac{A_{132}}{6D^2} r_1, \quad (10)$$

$$F_{\text{vdW}}(D) = -\frac{A_{132}}{6D^2} \left(\frac{r_1 r_2}{r_1 + r_2} \right), \quad (11)$$

where r_1 and r_2 are the radii of the spherical surfaces. When r_1 and r_2 are sufficiently larger than D , equations (10) and (11) can be derived from equation (9) by using Derjaguin approximation. When A_{132} , D , r_1 and r_2 are common in the equations (9), (10) and (11), and $r_1 = r_2$, the magnitude of the vdW force is flat-flat > flat-sphere > sphere-sphere.

In vdW interaction, Hamaker constant is an important factor. Hamaker constant is determined by the dielectric constants of the medium and two interacting objects. When the interacting particles are made of the same material, the Hamaker constant is always positive and the vdW interaction becomes attractive. In addition, the larger the dielectric constant difference between the particle and medium is, the larger the absolute value of the Hamaker constant is. Since the dielectric constant of metals

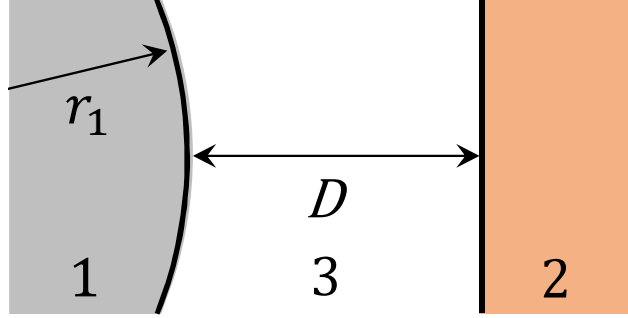


Figure 37. Spherical surface 1 and flat surface 2.

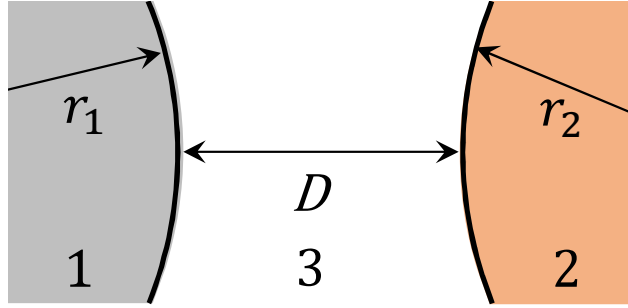


Figure 38. Spherical surfaces 1 and 2.

is much larger than that of dielectrics, Hamaker constant between metals in water is much larger than that between dielectrics. For example, the Hamaker constant between gold and gold and between silica and silica in water are $30 - 40 \times 10^{-20}$ J and 0.83×10^{-20} J, respectively [18]. Thus, the vdW attraction between gold particles in water is about 40 times larger than that between silica particles under the same conditions.

The thickness of the object also affects the magnitude of vdW interaction. vdW force per unit area working between flat objects with a flat surface layer (film thickness T and T') is expressed as follows (Figure 39).

$$f_{\text{vdW}}(D) = -\frac{1}{6\pi} \left[\frac{A_{232'}}{D^3} - \frac{\sqrt{A_{121}A_{32'3}}}{(D+T)^3} - \frac{\sqrt{A_{1'2'1'}A_{323}}}{(D+T')^3} + \frac{\sqrt{A_{1'2'1'}A_{121}}}{(D+T+T')^3} \right] \quad (12)$$

Figure 40 shows the effective Hamaker constant $A(L)$ between the parallel planes of polystyrene having a gold surface layer in water [31]. L is the distance between

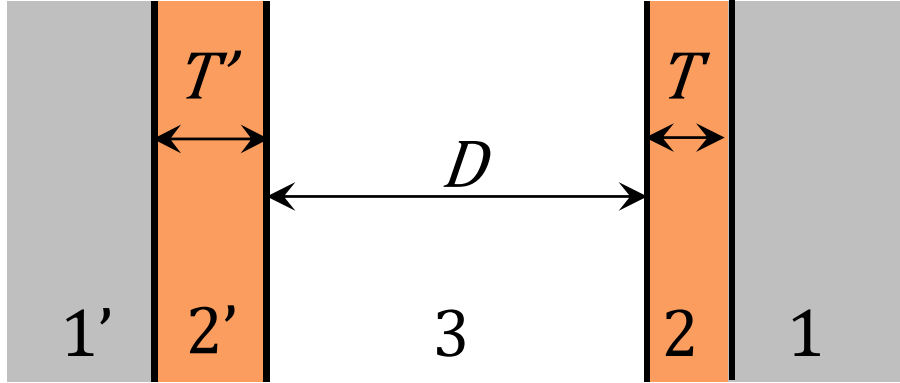


Figure 39. Interaction between two flat objects with a surface layer.

the surfaces of the planes and corresponds to D in equation (12). When the gold layer thickness is sufficiently smaller than L , $A(L)$ approaches the Hamaker constant between polystyrene objects. When the thickness is sufficiently larger than L , $A(L)$ approaches the Hamaker constant between gold objects. In particular, when the gold film thickness is approximately 100 nm, the effective Hamaker constant can be approximated with that of gold objects at $L < 20$ nm, where DLVO interaction generally plays an important role in water.

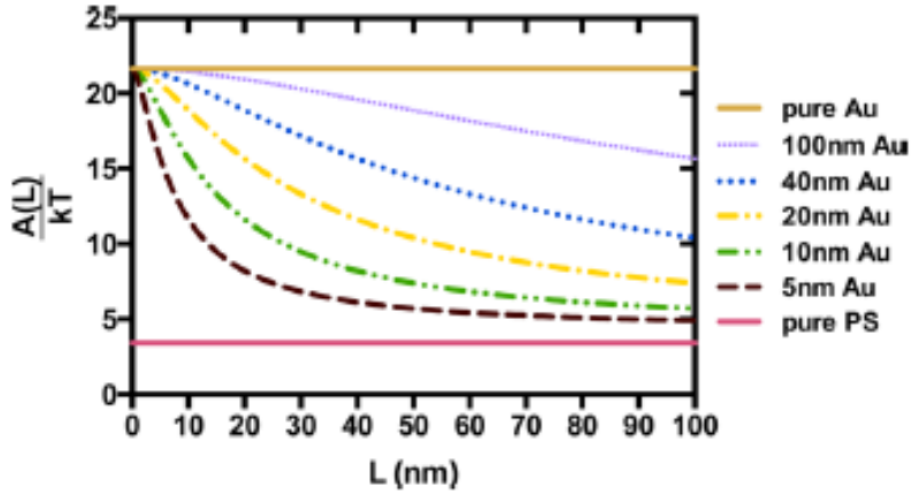


Figure 40. Effective Hamaker constant between parallel flat polystyrene with a gold surface layer in water [31].

1.1.2 Electric double layer repulsion

When the solid surface has a nonzero surface potential by the surface electric charge in liquid, ions in the liquid are attracted to or repelled from the solid surface, forming a layer of counterions against the surface charge. This layer is called an electric double layer (EDL). In an EDL a gradient of ion concentration forms near the solid surface (Figure 41), and the potential continuously approaches zero with the increase of distance from the solid surface.

The EDL repulsive force per unit area working between two identical solid planes in liquid is expressed as follows.

$$f_{\text{edl}} = \frac{\kappa^2}{2\pi} Z e^{-\kappa D} \quad (13)$$

$$Z = 64\pi\epsilon_0\epsilon(k_{\text{B}}T/e)^2 \tanh^2 (ze\psi_0/4k_{\text{B}}T), \quad (14)$$

where κ^{-1} , ϵ_0 , ϵ , e , z , and ϕ_0 are the Debye length, dielectric constant in vacuum, dielectric constant of liquid, the elementary charge, the valence of the ions, and the potential of the solid surfaces, respectively. The Debye length depends on the kind and concentration of electrolyte in liquid.

The equations of EDL repulsive force between the spherical and flat object and between the spherical objects are expressed as follows by using Derjaguin approximation.

$$F_{\text{edl}} = \kappa r_1 Z e^{-\kappa D} \quad (15)$$

$$F_{\text{edl}} = \kappa \frac{r_1 r_2}{r_1 + r_2} Z e^{-\kappa D} \quad (16)$$

1.1.3 vdW attraction vs. EDL repulsion

DLVO interaction working between colloidal particles of the same material is considered here. vdW attractive force is proportional to $1/D^3$ and EDL repulsive force is proportional to $e^{-\kappa D}$. DLVO potential, obtained from the sum of these forces, plotted with respect to the distance between surfaces D thus exhibits a characteristic profile. DLVO potential between the spherical particles of radii r_1 and r_2 is expressed

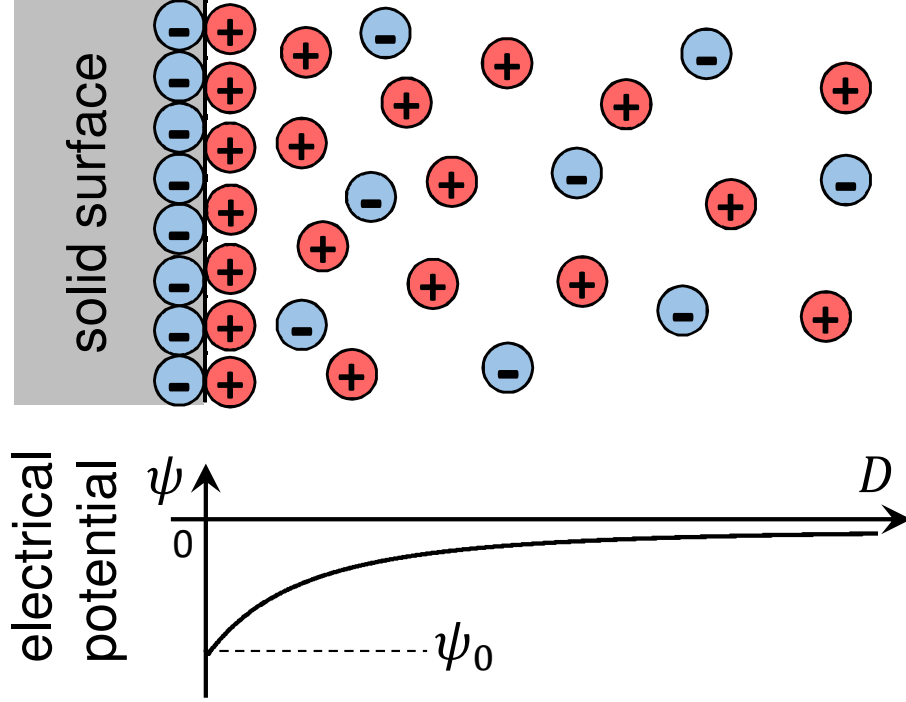


Figure 41. Schematic drawing of EDL and electric potential formed by surface potential in liquid.

by the following equation obtained by integrating the sum of equations (11) and (16) with respect to D .

$$W_{\text{DLVO}} = -\frac{A_{131}}{6D} \frac{r_1 r_2}{r_1 + r_2} + \frac{r_1 r_2}{r_1 + r_2} Z e^{-\kappa D}. \quad (17)$$

Figure 42 shows three characteristic profiles of DLVO potential between two particles of same materials in water dependent on salt concentration. Here $r_1 = 1 \mu\text{m}$, $r_2 = 0.5 \mu\text{m}$, $A_{131} = 10 \times 10^{-20} \text{ J}$, $T = 297 \text{ K}$, $\phi_0 = 40 \text{ mV}$, and the electrolyte is monovalent. When D is sufficiently small, vdW attractive force always exceeds EDL repulsive force. For solid particles, the hard body repulsion appears in the vicinity of the distance of 0, and DLVO potential has a primary minimum. When the salt concentration is low, a large energy barrier prevents the particles from the falling to the primary minimum. Increase of the salt concentration decreases the EDL repulsion, and at a moderate salt concentration, the potential has a secondary minimum deeper than $k_B T$ ($\simeq 4 \times 10^{-21} \text{ J}$ at room temperature). When salt concentration is

high, the energy barrier disappears and DLVO interaction become attractive at all distances.

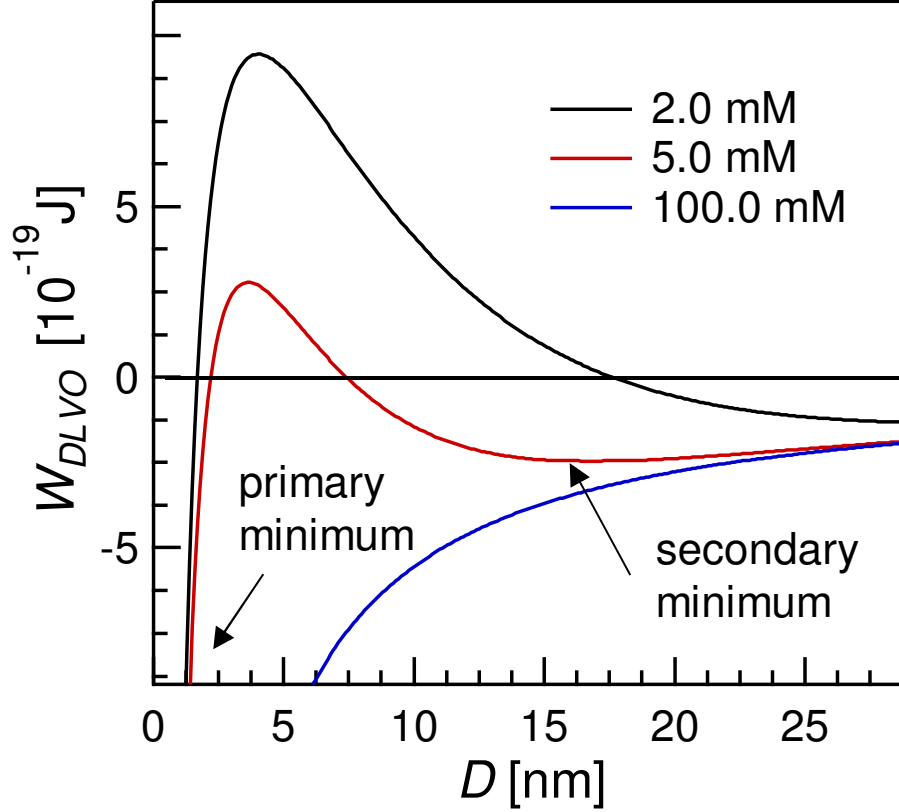


Figure 42. Salt concentration dependence of DLVO potential.

The differences in the DLVO potentials in Figure 42 also cause the difference in the aggregation / adsorption of particles and their mobility in the aggregated / adsorbed state. For the potential profile of a low salt concentration, see that of 2.0 mM in Figure 42, the particles stochastically crossing the energy barrier are trapped at the primary minimum. In addition, the particles cannot be trapped at the shallow secondary minimum at large D that is not deeper enough than $k_B T$. For the potential profile of moderate salt concentration, see that of 5.0 mM in Figure 42, the particles crossing the energy barrier are trapped at the primary minimum. In addition, particles can be stochastically trapped at the secondary minimum that is considerably deeper than $k_B T$. For the potential profile of a high salt concentration, see that of 100.0 mM in Figure 42, the particles rapidly aggregate by the attractive potential and

1 INTRODUCTION

are trapped at the primary minimum. When a particle is trapped on another object at a local minimum of DLVO potential, its mobility reflects whether the particle is at the primary or secondary minimum. At the primary minimum of the potential, where $D \simeq 0$, the surfaces possessing (at least) molecular-level roughness are tightly in contact, and thus the adsorbed particle at the minimum cannot exhibit thermal motion in general [18]. At the secondary minimum in the potential, where D has typically of the order of 1 to 10 nm, the potential profile is smooth and the influence of the microscopic surface roughness on the profile is small because of the distance. The particles can thus thermally move along the surface while remaining trapped at a secondary minimum when their surfaces are sufficiently smooth.

As can be seen from equations (14) and (17), the profile of DLVO potential also depends on the surface electric potential of particles and the Hamaker constant.

1.2 DLVO interaction of metallodielectric particle

Our metallodielectric particle (MDP) consisted of a spherical dielectric colloidal particle with one metal patch on its surface (Figure 43). We expect that anisotropic DLVO interaction works between metallodielectric particle and another object. As described above (Sec.1.1.1 of Chapter III), the Hamaker constant between metal surfaces is generally one order of magnitude larger than that between dielectric surfaces, and thus the vdW attraction between metal surfaces is larger than that between dielectric surfaces. When an MDP interacts with a metal and dielectric object, the vdW attraction between the metal patch and a metal object is larger than that between the patch and a dielectric object in vacuum (Figure 43). When the medium is a dielectric, both the relative magnitude and sign of the interaction depend on the dielectric constant of the medium. Nevertheless, the attraction is the largest between metal surfaces among these four combinations.

As described above (Sec.1.1.1 of Chapter III), it is possible to tune the vdW attraction between an MDP and bulky metal object so that it is stronger than that between two MDPs, by making their metal patch thin. By combining the tuning of this vdW attraction and that of EDL repulsion by surface charge and salt concentration, we expect that the anisotropy of the DLVO interaction between MDPs and/or between an MDP and bulk metal can be widely controlled from repulsion to attraction.

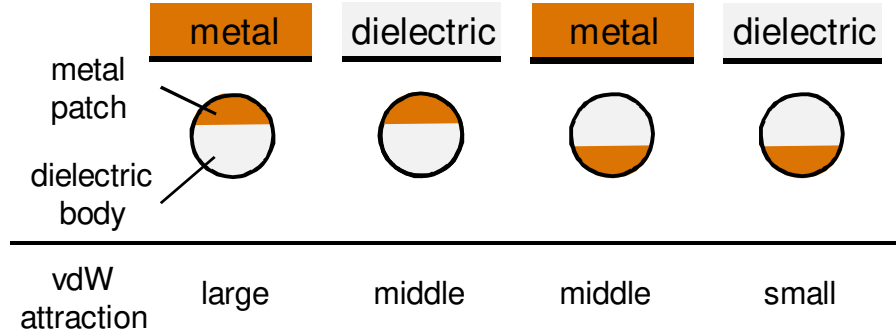


Figure 43. Comparison of the vdW attraction between an MDP and metal or dielectric surface in vacuum.

Such a control of interactions could realize, for example, a monolayer of MDPs on the surface of a metal object where the metal patches of the MDPs bond to the metal surface (Figure 44). As a result, a dielectric layer whose thickness is of the order of the diameter of colloidal particles is formed on the metal surface.

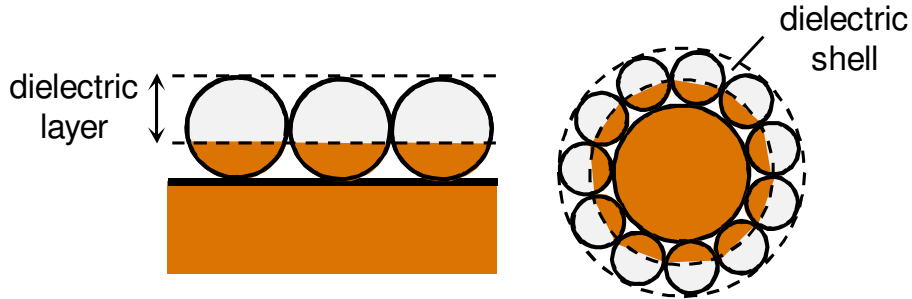


Figure 44. A monolayer of MDPs on a metal surface.

1.3 Motivation and purpose

Although Shemi and Solomon reported the characteristic self-assembled structures formed by the anisotropic DLVO interaction between MDPs [31], there have been no studies tuning the anisotropic DLVO interactions between multiple particles and objects, and realizing highly controlled adsorption behavior of MDPs so far as we know. In experimental studies of patchy particles, anisotropic interactions are often realized by introducing new interactions other than DLVO interaction. These interactions

2 EXPERIMENTAL SECTION

sometimes specify or limit the materials of the system and experimental methods. If highly controlled adsorption of colloidal particles is realized by the well-known, widely used DLVO interaction, it can be applied to various experimental systems for the introduction of anisotropic interactions to control the self-assembly or dispersed state of colloidal particles, being a new strategy in colloidal experiments.

We worked on realizing selective adsorption and structure formation of MDPs on metal surfaces. Au-silica patchy particles on which a small gold thin film (thickness was $\lesssim 10$ nm) was formed were used as MDPs. We investigated the salt concentration dependence of the adsorption behavior of the MDPs to 100 nm-thick gold films and glass surface.

2 Experimental section

To compare the adsorption behavior of MDPs on glass surfaces with that on Au surfaces, we first observed the dispersion state of MDPs on an Au-patterned substrate, which was a glass substrate patterned with a thick Au film on its surface. Next, the self-assembled structure of MDPs adsorbed on an Au surface was investigated in a dispersion of MDPs and large particles coated with a thick Au film. We observed a sample with an optical microscope (TE 2000-U, Nikon, Tokyo), with objective lenses (CFI S Plan Fluor ELWD 40 \times , CFI Plan Apo Lambda 60 \times Oil, and CFI Plan Fluor DLL 100 \times Oil). All experiments were performed at room temperature (approximately 25°C).

2.1 Preparation of MDPs

We first produced a close-packed monolayer of spherical silica particles (Hyprecica SS, UEXC, Tokyo, Japan) with a diameter of 1.5 μm following the method in Ref. [76]. The silica particles were monodisperse (coefficient of variation 2 %). Next, Au patches were formed on the surface of the particles by thermal deposition using the glancing angle deposition method [85,86]. The angle of the monolayer to the incident direction of evaporated metal, termed the monolayer angle, was small (5° or 10°). Various shapes of patches smaller than the silica hemisphere formed (Figure 45 (a)) because the patch shape depends on the orientation of the colloidal crystal domains

2 EXPERIMENTAL SECTION

and the monolayer was polycrystalline [85,86]. We deposited Cr followed by Au, and their thicknesses were respectively 3 and 10 nm when the evaporation angle to the particle surface is 90° . The thickness of a patch becomes smaller as evaporation angle to the particle surface deviates more from 90° (Figure 45 (b)) [87]. For the small monolayer angle described above, no metal was deposited on the particle surface at an evaporation angle of 90° ; the maximum patch thickness was at its edge closest to the evaporation source, where the evaporation angle to the surface is at its maximum, and the maximum thickness also depends on crystal orientation. For example, when the monolayer angle was 5° or 10° , the maximum thicknesses at the lower edges of the patches for the crystal orientation in Figure 45 (b) were geometrically estimated to be 5.6 and 7.6 nm, respectively. Thus, the Au patch of the MDPs was considerably smaller than the hemispherical surface and there was variation in the shape of the patches and non-uniformity in the thickness of a patches. Then, the surface of each Au patch was chemically modified with sodium 3-mercapto-1-propanesulfonate (98.7 wt%, Wako, Osaka, Japan) to provide negative dissociable groups. The particles were washed thoroughly with ethanol and then stored in ethanol [34].

2.2 Adsorption of MDPs to an Au-patterned substrate

An Au-patterned substrate was prepared by the same procedure as that used to fabricate the MDPs. A close-packed monolayer of spherical silica particles (Hyprecica TS, UEXC) with a diameter of $5.0\ \mu\text{m}$ was formed on a glass substrate. The silica particles were monodisperse (coefficient of variation 2 %). We deposited Cr (5 nm) followed by Au (100 nm) onto the monolayer at an angle of 90° . The particles were removed without surface modification. As a result, we obtained a honeycomb-like pattern of triangular Au films with a side length of approximately $2.5\ \mu\text{m}$ on the glass substrate (Figure 46 (a)). The number of triangular Au films was 9.2 pieces/ $100\ \mu\text{m}^2$. It is reported that an untreated gold surface is also negatively charged as the chemically modified MDPs, but the surface electrical potential of an untreated gold surface is much weaker than that of the surface with dissociable groups such as the MDPs [88].

Then, MDPs (0.02 vol%) prepared with a monolayer angle of 5° were dispersed in aqueous solutions of NaCl (99.5 %, Wako). NaCl concentrations were 0.0, 1.0, 3.0,

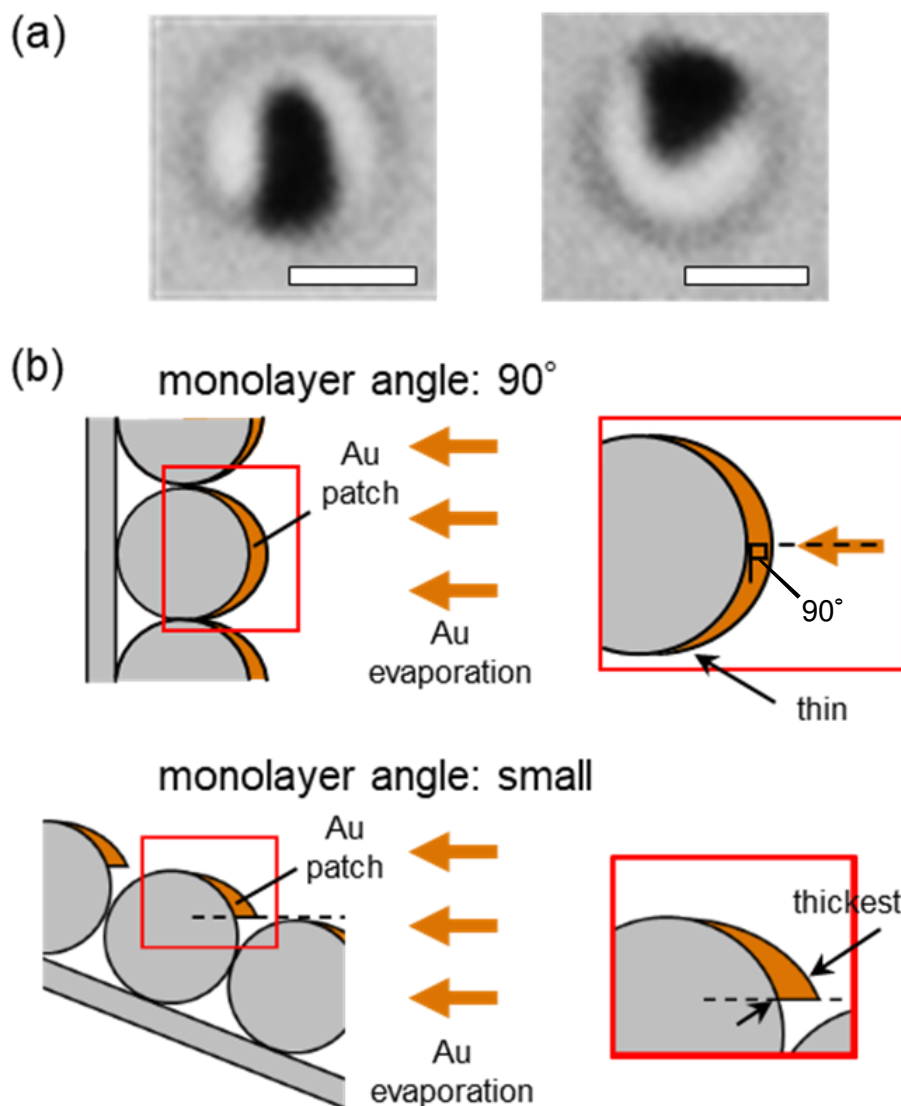


Figure 45. An MDP and its Au patch. (a) Optical microscope images of MDPs in mixtures with deposition monolayer angles of 5° and 10° dispersed in water. The Au patch appears dark. Scale bars, $1\ \mu\text{m}$. (b) Schematics of Au patch deposition on the monolayer of spherical particles. The monolayer angle is 90° for the upper row and less than 30° for the lower row.

and 5.0 mM. These dispersions were confined between the Au-patterned substrate and a glass cover slip with a silicone rubber spacer (thickness: 0.5 mm). The horizontal area where a dispersion was confined was approximately $10 \times 10\ \text{mm}$. In the cell, the sedimentation behavior of the MDPs was considered to be almost the same as that of spherical silica particles because the patch was very thin compared with the particle

2 EXPERIMENTAL SECTION

size, providing the sedimentation rate of $1.4 \mu\text{m/s}$ calculated with Stokes' law. At the concentration of the MDPs, the average number of MDPs was 5.7 particles/ $100 \mu\text{m}^2$ when all the particles had settled. The number ratio of sedimented MDPs to triangular Au films on the substrate was thus about 2:3.

Figure 46 (b) shows the experiment and observation procedure. The Au-patterned substrate was placed at the bottom of the cell. The dispersed MDPs sedimented toward the substrate. This state of the cell is called the normal state in the following. It takes 6 min for all MDPs to settle in the $500 \mu\text{m}$ -thick solution at the calculated sedimentation rate. The sedimented MDPs interacted with the Au-patterned substrate in the normal state. It is considered that the number of particles on the bottom substrate increases almost linearly with time during the 6 min sedimentation process. Considering the time that all MDPs interact with the Au-patterned substrate as the reaction time, the average number of MDPs interacting with the substrate in the 6 min is half of all the particles because the MDPs in sample are uniformly dispersed at first. Thus, the reaction time is regarded as 3 min. Next, the cell was flipped vertically, which is called the reversed state in the following. The non- and very weakly adsorbed MDPs left the Au-patterned substrate and sediment in the reversed state; only the adsorbed MDPs remained on the surface of the substrate. We observed the adsorbed particles under diffuse illumination from the top of the cell. The observation was conducted about 2 min after the reversal of the cell to ensure that the particles leaving the Au-patterned substrate had moved sufficiently away from the substrate. During this observation, only a few particles that detached from and left the substrate were observed; i.e. the adsorption of MDPs was reasonably stable. The reaction between the substrate and MDPs in the normal state and observation of the adsorbed particles in the reversed state were repeated four times and the time evolution of the adsorption of the MDPs was observed. The reaction time of each normal state was estimated considering the sedimentation time of MDPs. The reaction time was slightly different for each experiment, but the total reaction time was more than 20 min at the fourth observation for all the experiments.

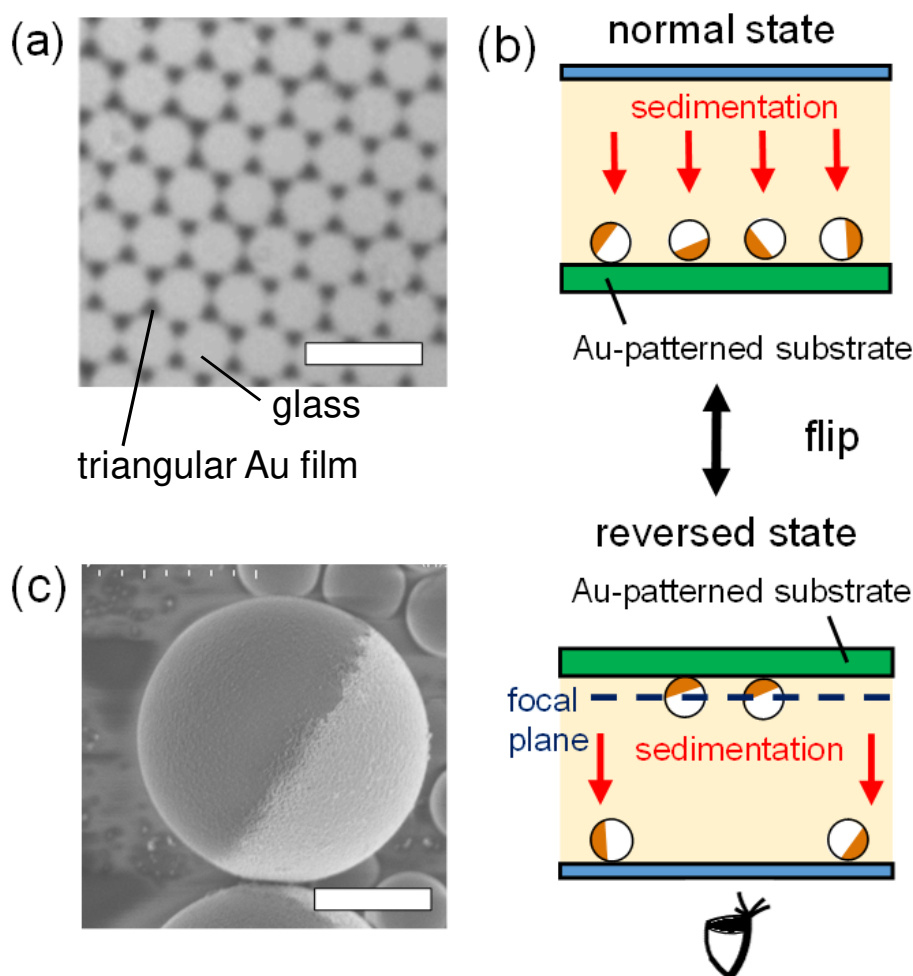


Figure 46. Au-patterned substrate, experimental method, and large particle. (a) Optical microscopy image of an Au-patterned substrate. The dark spots are the triangular Au films on the glass substrate. Scale bar is $10\ \mu\text{m}$. (b) Schematic of MDP adsorption to an Au-patterned substrate. (c) Scanning electron microscopy image of a large particle with a thick hemispherical Au film. The bright part is the Au film and the darker part is the silica surface. Scale bar is $2\ \mu\text{m}$.

2.3 Adsorption of MDPs to half Au-coated large particles

The particles with a diameter of $5.0\ \mu\text{m}$ that were employed in the production of the Au-patterned substrate were then used as the large Janus particles possessing a thick Au hemispherical film with a thickness at the film center of $100\ \text{nm}$ (Figure 46c). These large particles were dispersed in NaCl aqueous solutions together with a

3 RESULTS AND DISCUSSION

mixture of MDPs prepared with monolayer angles of 5° and 10° . The number of the large particles and that of MDPs in the samples were equivalent. The concentrations of the MDP mixture and large particles were 0.03 and 0.01 vol%, respectively. The NaCl concentrations were 1.0, 3.0, and 5.0 mM. Each dispersion was confined in a cell with dimensions of $10 \times 10 \times 0.5$ mm using two glass cover slips and a 0.5 mm-thick silicone rubber spacer. The MDPs and large particles settled on the bottom of the sample cell and dispersed two-dimensionally. The particles were observed from the bottom side of the cell 1 h after preparation of the dispersion.

3 Results and discussion

3.1 Adsorption of MDPs to Au-patterned substrate

First, we describe the results for the dispersion state of MDPs on the Au-patterned substrate. The experiments with different salt concentrations from 0.0 to 5.0 mM revealed that the adsorption of MDPs to the Au-patterned substrate strongly depended on salt concentration. Figure 47 (a) displays the microscope images obtained for the fourth reversed state; that is, the reaction time between the MDPs and substrate was more than 20 min and the adsorption was speculated to have reached the steady state (as discussed later). When the salt concentration was low (0.0 and 1.0 mM), few MDPs were adsorbed on the Au-patterned substrate. When the salt concentration was high (3.0 and 5.0 mM), many MDPs were adsorbed on the triangular Au films on the substrate. Figure 47 (b) shows the marked increase of the number of MDPs adsorbed on the substrate at the fourth observation of the reversed state with increasing salt concentration. Next, the proportions of the particles adsorbed on the Au films and glass surface with respect to all the adsorbed MDPs was estimated from the images for the systems with salt concentrations of 3.0 and 5.0 mM. We found that, in 318 particles observed for this analysis, 92 % of MDPs obviously adsorbed on the Au films and 3 % to the glass surface; 5 % of particles were near the edges of the Au films and we were unable to clearly distinguish the adsorbing region. Because there were much fewer MDPs on the glass surface than on the Au films, most of the particles near the edges of the Au films were presumed to be adsorbed on the films rather than the glass surface.

3 RESULTS AND DISCUSSION

The thermal motion of the MDPs adsorbed on Au films was observed at any salt concentrations used. Figure 47 (c) depicts the trajectories of the MDPs for 3 s in a dispersion with a salt concentration of 5.0 mM. There are apparent differences in the mobilities of the particles; some of them were almost immobile, whereas others moved around on a triangular Au film while remaining attached to it. Figure 47 (d) shows the frequency distribution of the standard deviation σ of the distance from the averaged position in a 3 s trajectory of a particle, that is, the radius of gyration, at salt concentrations of 3.0 and 5.0 mM. The first peaks for the dispersions with salt concentrations of 3.0 and 5.0 mM appeared at σ of $\sim 0.04 \mu\text{m}$. These particles are the immobile particles, which did not appear to move during the observation, and their small but non-zero σ is predominantly caused by the apparent positional fluctuation resulting from the noise in the images. In contrast, there were mobile particles exhibiting remarkably larger σ than the first peak. We classified particles with $\sigma < 0.10 \mu\text{m}$ as immobile. The calculated ratios of immobile particles to all adsorbed particles were 0.81 and 0.50 for dispersions with salt concentrations of 3.0 and 5.0 mM, respectively (cf. Figure 47 (d)). These ratios were similar for the other observations described later.

The dependence of the number of adsorbed particles and their different mobilities on salt concentration described above can be explained by considering DLVO interactions (cf. Sec.1.1.3 of Chapter III). Colloidal particles exhibiting DLVO interactions with each other aggregate through vdW attraction when EDL repulsion is suppressed with increasing salt concentration. In our system, selective adsorption of MDPs to the Au film on a glass substrate should be driven by the strong vdW attraction between Au surfaces, and the increasing number of adsorbed particles with salt concentration can be explained by the suppression of EDL repulsion. The difference in the mobility of MDPs is considered to reflect whether the particles are at the primary or secondary minimum of the interaction potential. The larger ratio of the mobile to immobile particles in the dispersion with a salt concentration of 5.0 mM than that for the case of 3.0 mM is probably because the secondary minimum became deeper at higher salt concentration, so the particles were more likely to be trapped there and exhibited mobility.

Next, the dependence of the number of the adsorbed particles on reaction time was investigated (Figure 47 (e)). The results for dispersions with salt concentrations of

3 RESULTS AND DISCUSSION

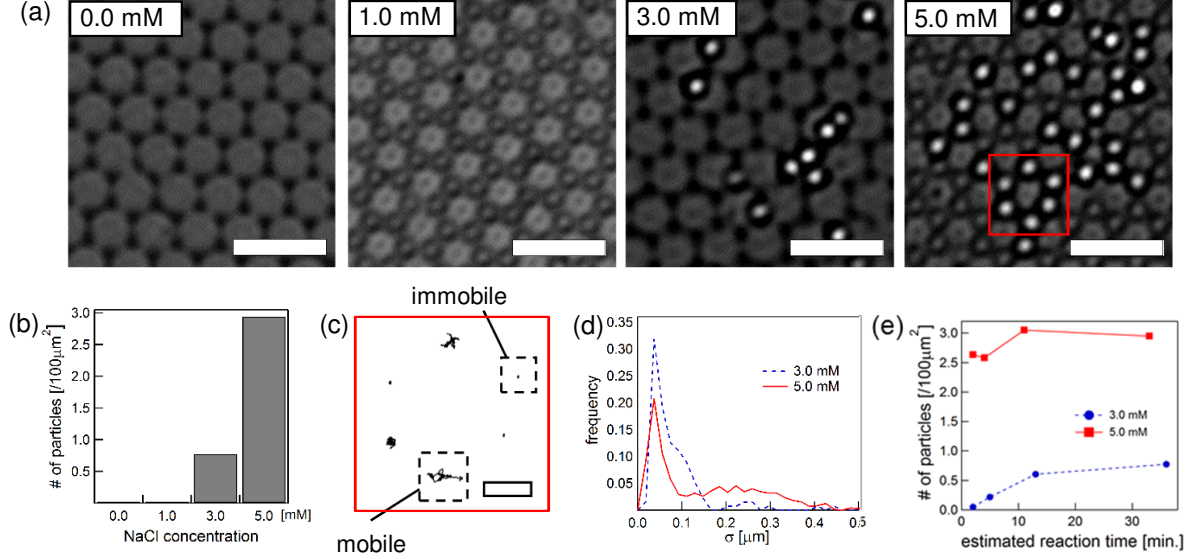


Figure 47. Adsorption of MDPs on Au-patterned substrates. (a) Optical microscope images of Au-patterned substrates after the particle adsorption reached a steady state (reaction time > 20 min). Salt concentrations are indicated on each panel. The center of an MDP appeared bright and there were no adsorbed particles for the dispersions with salt concentrations of 0.0 and 1.0 mM. The slight difference in the appearance of triangular Au films between the images is an artifact caused by the different focal positions. Scale bars, 10 μm . (b) Dependence of the number density of MDPs adsorbed on an Au-patterned substrate after the adsorption reached steady state (reaction time > 20 min) on salt concentration. The density was calculated from the observation of $\geq 45000 \mu\text{m}^2$ of Au-patterned substrate. The calculated density has an error of about $\pm 10\%$ because of the heterogeneity in the spatial distributions of MDPs. (c) The trajectories of the centers of six MDPs over 3 s, corresponding to the region inside the red square in the panel for the dispersion with a salt concentration of 5.0 mM in (a). Scale bar, 1 μm . (d) Frequency distribution of the gyration radius of the trajectories σ of the adsorbed MDPs at a reaction time of ≥ 30 min for dispersions with salt concentrations of 3.0 and 5.0 mM. The numbers of particles analyzed were 135 and 728 for dispersions with salt concentrations of 3.0 and 5.0 mM, respectively. (e) Dependence of the number density of adsorbed MDPs on the estimated reaction time for dispersions with salt concentrations of 3.0 and 5.0 mM. The densities for dispersions with salt concentrations of 0.0 and 1.0 mM were stochastically unreliable because of the few adsorbed particles; thus, the data for these dispersions were omitted.

3 RESULTS AND DISCUSSION

0.0 and 1.0 mM are not presented here because only a few adsorbed particles were observed. For dispersions with salt concentrations of 3.0 and 5.0 mM, the number of adsorbed particles tended to increase over time and almost reached the steady-state value at around 10 min, considering that the estimated density had an error of about $\pm 10\%$. The more apparent dependence on reaction time for the dispersion with a salt concentration of 3.0 mM than that for the 5.0 mM dispersion can again be explained by the DLVO potential. That is, the adsorption for the dispersion with a salt concentration of 3.0 mM was predominantly at the primary minimum and thermal activation to surmount the potential barrier was required; in contrast, there was no barrier for the adsorption at the secondary minimum.

Different from the dependence of the adsorption state on salt concentration, the reaction-time dependence of the adsorption state could not be explained by only the DLVO interaction. In the fourth observation in Figure 47 (e), the reaction time was more than 30 min; i.e. more than twice the time needed to reach steady-state adsorption. However, many bare triangular Au films on the substrate and dispersed non-adsorbed MDPs remained in the system (cf. Figure 47 (b) and (e)). When all the particles were adsorbed as described above, the number of particles was $5.7/100\ \mu\text{m}^2$, so about half of the particles were not adsorbed on to the substrate even in the dispersion with a salt concentration of 5.0 mM, where $2/3$ of the triangular Au films were unoccupied because there were $9.2\ \text{films}/100\ \mu\text{m}^2$. If the adsorption of MDPs to an Au film was an ordinary stochastic process, the number of adsorbed particles should keep increasing because there were numerous non-adsorbed MDPs and unoccupied Au films. In addition, the ratio of immobile to mobile particles did not depend on the reaction time. If the relaxation of the adsorbed state from the secondary to primary minimum is also stochastic, the ratio of the immobile to mobile particles should increase, at least, after the number of adsorbed particles reaches a steady value.

The difference between this simple expectation based on the DLVO interaction and the experimental results suggests that, at the same salt concentration, there are MDPs that are readily adsorbed on the Au films at the primary minimum, MDPs that are readily adsorbed at the secondary minimum, and MDPs that are difficult to be adsorbed. We speculate that a cause of this difference in the adsorption behavior is the variations in the thickness and shape of the Au patches of MDPs. When a

3 RESULTS AND DISCUSSION

patch is thick, the vdW attractive force becomes large, so the secondary minimum becomes deep and the adsorption at the minimum should be stabilized. A thick patch also makes the potential barrier between the primary and secondary minima low, facilitating the adsorption at the primary minimum. Although the influence of the variation of the patch shape on the adsorption behavior and state is unclear, it should affect their dynamics. The wide distribution in the thermal mobility of the MDPs in the dispersion with a salt concentration of 5.0 mM in Figure 47 (d) might reflect the variation of patch shape in addition to the stochastic fluctuations.

3.2 Adsorption of MDPs to thick Au films on large particles

This section describes the adsorption behavior of MDPs to large particles possessing a thick Au hemispherical film. Figure 48 (a) shows the dispersions of MDPs and large particles. The Au film on the large particle faced downward and thus the particle appeared to be black, because the hemispherical Au film was thick and heavy. For the dispersion with a salt concentration of 1.0 mM, almost no adsorption of MDPs to large particles was observed. In contrast, for dispersions with salt concentrations of 3.0 and 5.0 mM, substantial adsorption of MDPs to the Au hemispheres of the large particles was observed; the Au hemispheres were surrounded by a monolayer of MDPs. This dependence of the adsorption of the MDPs to thick Au films on salt concentration qualitatively agrees with that observed for the Au-patterned substrates described in Sec.3.1 of Chapter III. The Au patches of the adsorbed MDPs were not observable in the images; that is, they overlapped with the large particles when observed from the bottom of the cell. This means that the Au patch of MDPs was adsorbed on the Au film of the large particles, as shown in Figure 48 (b), as expected because of the strong vdW attraction between Au surfaces. In addition, because the silica surfaces of the MDPs faced outward, the dispersed MDPs cannot be adsorbed to the MDPs forming the monolayer on the large particle. The characteristic structure formed by the interaction of Au surfaces is more evident for the large particles with a patterned Au film (Figure 48 (c)). These patterned films were produced by chance because of the overlap of the particles during the metal deposition process (cf. Sec.2.1 of Chapter III). Figure 48 (c) reveals that MDPs were adsorbed selectively on the patterned Au film of the large particles, where MDPs followed the thermal motion of the patterned

3 RESULTS AND DISCUSSION

film; i.e. they were adsorbed stably.

For the dispersions with salt concentrations of 3.0 and 5.0 mM, we observed 320 and 340 MDPs adsorbed to large particles, respectively, and none of the MDPs detached from the large particles during the ~ 10 s of observation. In addition, the coverage of the large particles with MDPs was high in these systems. The stable adsorption and high coverage of MDPs indicate that the adsorption energy was considerably larger than the thermal energy. In addition, most of the adsorbed MDPs showed thermal fluctuations in position and direction, indicating that they were at the secondary minimum of the DLVO potential.

For the dispersion with a salt concentration of 5.0 mM, where the EDL repulsion was most screened under our experimental conditions, the adsorption between the patches of MDPs, i.e. formation of MDP clusters, was also observed (Figure 48 (a)). The dissociation of MDP clusters was also observed, and thus MDP monomers coexisted with the clusters. This behavior is different from the fairly stable adsorption between MDPs and large particles described above. Obvious MDP-MDP adsorption was seldom observed in the dispersion with a salt concentration of 3.0 mM (Figure 48 (a)). For the dispersion with a salt concentration of 1.0 mM, although the MDP density was higher than those for the cases of 3.0 and 5.0 mM in the observed region in Figure 48 (a), neither MDP-large particle nor MDP-MDP adsorption was observed. These observations indicate that we succeeded in suppressing the adsorption between MDPs while selective adsorption between the patches of MDPs and thick Au films of the large particles was induced. Such selectivity was realized by making the vdW attraction between MDPs and the large particles stronger than that between MDPs by making the Au patch of MDPs thinner than that of the large particles and by increasing the EDL repulsion between MDPs through surface modification.

The observed adsorption behavior where most MDPs are adsorbed to the thick Au films at the secondary minimum of the DLVO potential is different from the adsorption of the MDPs to the Au-patterned substrate at the same salt concentration. This difference may be related to the non-uniformity of the Au film thickness of the large particles and its curvature. Because the hemispherical Au film faced downward in the reaction cell, MDPs could not be adsorbed on the thickest part of the Au film (100 nm thick at the film center) (Figure 48 (b)). An adsorbed MDP with a diameter of 1.5 μm was in contact with a large particle with a diameter of 5.0 μm at an

angle of $\sim 57^\circ$ from the bottom of the particle. Although the orientation of the large particles thermally fluctuated, the Au film thickness at 57° from the center of the film was 40 nm, which was smaller than the film thickness of the Au-patterned substrate (100 nm). In addition, the vdW attraction between spherical surfaces is weaker than that between spherical and flat surfaces [18]. These differences in the thickness and curvature of interacting surfaces weakened the attraction in the MDP-large particle systems, and thus the adsorbed MDPs at the secondary potential minimum found it difficult to relax to the primary minimum.

4 Summary

In this study, we realized highly selective adsorption of one-patch MDPs, where the Au patch of the particle were adsorbed only on the bulk-like Au surface and not to Au patches of other MDPs, by controlling the anisotropy of the DLVO interaction via the thickness and surface charge of the Au patches of MDPs. We observed that MDPs were adsorbed on thick Au films on a glass substrate but not to the dielectric (glass) surface. The adsorbed MDPs exhibited different kinetic states, almost immobile and thermally mobile, which were considered to correspond to adsorption at the primary and secondary minima of the DLVO potential, respectively. Under similar conditions, MDPs were adsorbed on a thick Au film on large particles and formed a fairly densely packed monolayer of MDPs with their Au patches facing the large particle. That is, we succeeded in forming a solid dielectric shell on the surface of metal particles. In general, the vdW attraction between metal surfaces is very strong compared with that between dielectric surfaces. In addition, the DLVO interaction between colloidal particles has been studied extensively, such as its dependence upon various physical properties of particles and media and how it affects the kinetics of aggregation/condensation. Our study demonstrating highly controlled self-assembly by tuning the anisotropy of DLVO interactions using a metal patch is therefore useful for controlling self-assembly in nano/microparticle systems to develop functional materials. For example, hybrid colloidal particles composed of multiple materials inherently display anisotropic DLVO interactions, which makes them an ideal building block to fabricate nano/microstructured hybrid materials.

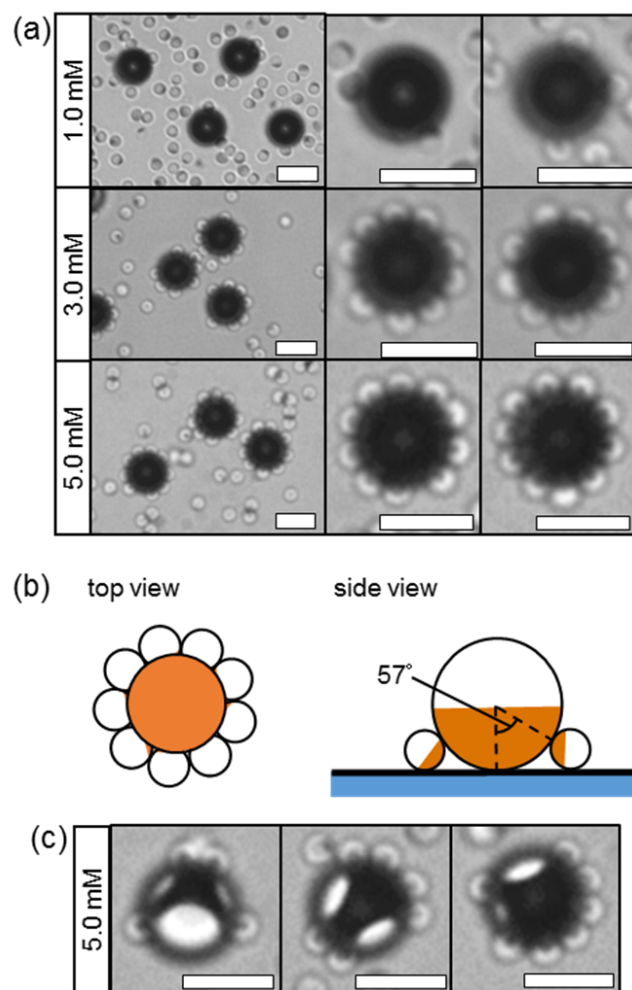


Figure 48. Dispersion of MDPs and large particles with a thick hemispherical Au film. (a) Optical microscopy images of samples observed 1 h after preparation. The difference in the appearance of MDPs between images is an artifact caused by the slightly different focal positions. (b) Schematics of a large particle coated with MDPs. (c) Adsorption of MDPs to large particles with a patterned Au patch observed 2 h after sample preparation. The patterned Au patches are on the bottom hemispheres of the large particles. Scale bars, 5 μm . Salt concentrations are indicated in the panels.

Chapter IV

Concluding remarks

Our study on the structure formation in the amphiphilic Janus particles (AJPs)-water-oil ternary system elucidated for the first time the dependence of self-assembled structures on the composition of the system in single particle level and the structure formation mechanism. When the volume of the minority liquid phase (water) is smaller than the volume of AJPs, the formed structure reflects the amphiphilic structure of the particle as known in amphiphilic molecular systems. When the volume of the minority liquid phase is sufficiently larger than the volume of AJP, spherical droplets are formed by the same formation mechanism as typical Pickering emulsions, and AJPs behave as “ideal surfactant” so that all the particles are adsorbed on the water-oil interface. This self-assembly by the amphiphilicity of colloidal particles would be useful to create spatially heterogeneous mesoscopic structures and even new ordered phases could form with these particles in the future.

We also succeeded in realizing selective adsorption of metallodielectric patchy particles (MDPs) to a metal surface by inducing the anisotropy in DLVO interaction via a metal patch. Our study demonstrated that the adsorption behavior of an MDP to a metal surface can be tuned by controlling the film thickness of a metal patch, surface charge, and salt concentration of the solvent. We also succeeded in forming the protective particle layer on a metal surface using this selective adsorption. The attachment of metal patches to particles and modification of surface charge used in our study are simple and can be applied to wide range of micro- and nanoparticle systems. Therefore, it is expected that our method is useful to design colloidal molecules with desired interaction anisotropy, which are highly required to use the particles as a model experimental system to study phase behaviors of condensed system. In addition, such colloidal molecules are useful to produce tailor-made self-assembled structures of functional fine particles, highly required in nanotechnology to produce new and useful nano/microstructured materials for future applications.

Acknowledgment

Without the support of numerous individuals, the completion of this thesis would not have been possible and I am grateful for all of their support. First of all, I would like to thank professor Yasuyuki Kimura and professor Yasutaka Iwashita for their guidance over the past six years. Professor Yasuyuki Kimura introduced me to the world of colloids and soft matter. Professor Yasutaka Iwashita introduced me to the Janus particles and anisotropic particles. They are supportive, patient and always there to help when I experience difficulties in my research. Their dedication and enthusiasm to science inspires me and keeps me motivated for the next big challenge. I also would like to thank my thesis committee members professor Jun-ichi Fukuda and professor Shio Inagaki.

Finally, I want to thank my parents for their patience, and for supporting and encouraging me to pursue my dreams without reservation.

References

- [1] K. J. Lee, J. Yoon, and J. Lahann. Recent advances with anisotropic particles. *Curr. Opin. Colloid In.*, **16**(3):195–202, 2011.
- [2] A. Perro, S. Reculosa, S. Ravaine, E. B. Bourgeat-Lami, and E. Duguet. Design and synthesis of Janus micro- and nanoparticles. *J. Mater. Chem.*, **15**(35-36):3745–3760, 2005.
- [3] A. Walther and A. H. E. Mueller. Janus particles. *Soft Matter*, **4**(4):663–668, 2008.
- [4] M. Lattuada and T. A. Hatton. Synthesis, properties and applications of Janus nanoparticles. *Nano Today*, **6**(3):286–308, 2011.
- [5] T. Nousiainen. Optical modeling of mineral dust particles: A review. *J. Quant. Spectrosc. Radiat. Transf.*, **110**(14-16):1261–1279, 2009.
- [6] W. Wei, R. Minullina, E. Abdullayev, R. Fakhrullin, D. Mills, and Y. Lvov. Enhanced efficiency of antiseptics with sustained release from clay nanotubes. *RSC Adv.*, **4**(1):488–494, 2014.
- [7] L. Soler, V. Magdanz, V. M. Fomin, S. Sanchez, and O. G. Schmidt. Self-Propelled Micromotors for Cleaning Polluted Water. *ACS Nano*, **7**(11):9611–9620, 2013.
- [8] S. C. Glotzer and M. J. Solomon. Anisotropy of building blocks and their assembly into complex structures. *Nat. Mater.*, **6**(8):557–562, 2007.
- [9] S. Granick, S. Jiang, and Q. Chen. Janus particles. *Phys. Today*, **62**(7):68–69, 2009.
- [10] N. D. Burrows, A. M. Vartanian, N. S. Abadeer, E. M. Grzincic, L. M. Jacob, W. Lin, J. Li, J. M. Dennison, J. G. Hinman, and C. J. Murphy. Anisotropic Nanoparticles and Anisotropic Surface Chemistry. *J. Phys. Chem. Lett.*, **7**(4):632–641, 2016.
- [11] Q. Chen, J. K. Whitmer, S. Jiang, S. C. Bae, E. Luijten, and S. Granick. Supracolloidal Reaction Kinetics of Janus Spheres. *Science*, **331**(6014):199–202, 2011.
- [12] A. Kumar, B. J. Park, F. Tu, and D. Lee. Amphiphilic Janus particles at fluid interfaces. *Soft Matter*, **9**(29):6604–6617, 2013.
- [13] L. Hong, A. Cacciuto, E. Luijten, and S. Granick. Clusters of charged Janus

References

- spheres. *Nano Lett.*, **6**(11):2510–2514, 2006.
- [14] H.-R. Jiang, N. Yoshinaga, and M. Sano. Active Motion of a Janus Particle by Self-Thermophoresis in a Defocused Laser Beam. *Phys. Rev. Lett.*, **105**(26):268302, 2010.
- [15] D. Nishiguchi and M. Sano. Mesoscopic turbulence and local order in Janus particles self-propelling under an ac electric field. *Phys. Rev. E*, **92**(5):052309, 2015.
- [16] J. Zhang, B. A. Grzybowski, and S. Granick. Janus Particle Synthesis, Assembly, and Application. *Langmuir*, **33**(28):6964–6977, 2017.
- [17] Y. Wang, A. D. Hollingsworth, S. K. Yang, S. Patel, D. J. Pine, and M. Weck. Patchy Particle Self-Assembly via Metal Coordination. *J. Am. Chem. Soc.*, **135**(38):14064–14067, 2013.
- [18] J. N. Israelachvili. *Intermolecular and surface forces*, 2nd. ed. Academic Press Inc.: San Diego, 1991.
- [19] G. L. Hunter and E. R. Weeks. The physics of the colloidal glass transition. *Rep. Prog. Phys.*, **75**(6):066501, 2012.
- [20] S. C. Glotzer. Some assembly required. *Science*, **306**(5695):419–420, 2004.
- [21] Q. Chen, J. Yan, J. Zhang, S. C. Bae, and S. Granick. Janus and Multiblock Colloidal Particles. *Langmuir*, **28**(38):13555–13561, 2012.
- [22] J. Russo, P. Tartaglia, and F. Sciortino. Association of limited valence patchy particles in two dimensions. *Soft Matter*, **6**(17):4229–4236, 2010.
- [23] F. Sciortino, A. Giacometti, and G. Pastore. A numerical study of one-patch colloidal particles: from square-well to Janus. *Phys. Chem. Chem. Phys.*, **12**(38):11869–11877, 2010.
- [24] F. Romano and F. Sciortino. Two dimensional assembly of triblock Janus particles into crystal phases in the two bond per patch limit. *Soft Matter*, **7**(12):5799–5804, 2011.
- [25] R. Fantoni, A. Giacometti, F. Sciortino, and G. Pastore. Cluster theory of Janus particles. *Soft Matter*, **7**(6):2419–2427, 2011.
- [26] G. Munao, Z. Preisler, T. Vissers, F. Smallenburg, and F. Sciortino. Cluster formation in one-patch colloids: low coverage results. *Soft Matter*, **9**(9):2652–2661, 2013.
- [27] T. Vissers, Z. Preisler, F. Smallenburg, M. Dijkstra, and F. Sciortino. Predicting

- crystals of Janus colloids. *J. Chem. Phys.*, **138**(16):164505, 2013.
- [28] Z. Preisler, T. Vissers, F. Smalenburg, G. Munao, and F. Sciortino. Phase Diagram of One-Patch Colloids Forming Tubes and Lamellae. *J. Phys. Chem. B*, **117**(32):9540–9547, 2013.
- [29] F. Smalenburg and F. Sciortino. Liquids more stable than crystals in particles with limited valence and flexible bonds. *Nat. Phys.*, **9**(9):554–558, 2013.
- [30] Q. Chen, S. C. Bae, and S. Granick. Directed self-assembly of a colloidal kagome lattice. *Nature*, **469**(7330):381–384, 2011.
- [31] O. Shemi and M. J. Solomon. Effect of Surface Chemistry and Metallic Layer Thickness on the Clustering of Metallo-dielectric Janus Spheres. *Langmuir*, **30**(51):15408–15415, 2014.
- [32] L. Hong, A. Cacciuto, E. Luijten, and S. Granick. Clusters of amphiphilic colloidal spheres. *Langmuir*, **24**(3):621–625, 2008.
- [33] C. Yu, J. Zhang, and S. Granick. Selective Janus Particle Assembly at Tipping Points of Thermally Switched Wetting. *Angew. Chem. Int. Edit.*, **53**(17):4364–4367, 2014.
- [34] Y. Iwashita and Y. Kimura. Stable cluster phase of Janus particles in two dimensions. *Soft Matter*, **9**(45):10694–10698, 2013.
- [35] S. Sacanna, W. T. M. Irvine, P. M. Chaikin, and D. J. Pine. Lock and key colloids. *Nature*, **464**(7288):575–578, 2010.
- [36] Y. Wang, Y. Wang, D. R. Breed, V. N. Manoharan, L. Feng, A. D. Hollingsworth, M. Weck, and D. J. Pine. Colloids with valence and specific directional bonding. *Nature*, **491**(7422):51–61, 2012.
- [37] A. H. Groeschel, A. Walther, T. I. Loebling, F. H. Schacher, H. Schmalz, and A. H. E. Mueller. Guided hierarchical co-assembly of soft patchy nanoparticles. *Nature*, **503**(7475):247–251, 2013.
- [38] X. Mao, Q. Chen, and S. Granick. Entropy favours open colloidal lattices. *Nat. Mater.*, **12**(3):217–222, 2013.
- [39] F. Sciortino, A. Giacometti, and G. Pastore. Phase Diagram of Janus Particles. *Phys. Rev. Lett.*, **103**(23):237801, 2009.
- [40] G. Munao, D. Costa, A. Giacometti, C. Caccamo, and F. Sciortino. Structure and phase behavior of colloidal dumbbells with tunable attractive interactions. *Phys. Chem. Chem. Phys.*, **15**(47):20590–20599, 2013.

- [41] Z. Preisler, T. Vissers, G. Munao, F. Smalenburg, and F. Sciortino. Equilibrium phases of one-patch colloids with short-range attractions. *Soft Matter*, **10**(28):5121–5128, 2014.
- [42] A. Giacometti, C. Goegelein, F. Lado, F. Sciortino, S. Ferrari, and G. Pastore. From square-well to Janus: Improved algorithm for integral equation theory and comparison with thermodynamic perturbation theory within the Kern-Frenkel model. *J. Chem. Phys.*, **140**(9):094104, 2014.
- [43] Z. Preisler, T. Vissers, F. Smalenburg, and F. Sciortino. Crystals of Janus colloids at various interaction ranges. *J. Chem. Phys.*, **145**(6):064513, 2016.
- [44] F. Romano and F. Sciortino. Patterning symmetry in the rational design of colloidal crystals. *Nat. Commun.*, **3**:975, 2012.
- [45] B. P. Binks. Particles as surfactants - similarities and differences. *Curr. Opin. Colloid Interface Sci.*, **7**(1-2):21–41, 2002.
- [46] Y. Chevalier and M.-A. Bolzinger. Emulsions stabilized with solid nanoparticles: Pickering emulsions. *Colloid Surf. A-Physicochem. Eng. Asp.*, **439**:23–34, 2013.
- [47] C. Zeng, H. Bissig, and A. D. Dinsmore. Particles on droplets: From fundamental physics to novel materials. *Solid State Commun.*, **139**(11-12):547–556, 2006.
- [48] B. Abismail, J. P. Canselier, A. M. Wilhelm, H. Delmas, and C. Gourdon. Emulsification by ultrasound: drop size distribution and stability. *Ultrason. Sonochem.*, **6**(1-2):75–83, 1999.
- [49] S. U. Pickering. Emulsions. *J. Chem. Soc.*, **91**(2):2001–2021, 1907.
- [50] E. Dickinson. Food emulsions and foams: Stabilization by particles. *Curr. Opin. Colloid Interface Sci.*, **15**(1-2):40–49, 2010.
- [51] S. Tcholakova, N. D. Denkov, and A. Lips. Comparison of solid particles, globular proteins and surfactants as emulsifiers. *Phys. Chem. Chem. Phys.*, **10**(12):1608–1627, 2008.
- [52] B. S. Murray and R. Ettelaie. Foam stability: proteins and nanoparticles. *Curr. Opin. Colloid Interface Sci.*, **9**(5):314–320, 2004.
- [53] R. Aveyard, J. H. Clint, and T. S. Horozov. Aspects of the stabilisation of emulsions by solid particles: Effects of line tension and monolayer curvature energy. *Phys. Chem. Chem. Phys.*, **5**(11):2398–2409, 2003.
- [54] B. P. Binks and S. O. Lumsdon. Influence of particle wettability on the type and stability of surfactant-free emulsions. *Langmuir*, **16**(23):8622–8631, 2000.

References

- [55] A. D. Dinsmore, M. F. Hsu, M. G. Nikolaides, M. Marquez, A. R. Bausch, and D. A. Weitz. Colloidosomes: Selectively permeable capsules composed of colloidal particles. *Science*, **298**(5595):1006–1009, 2002.
- [56] R. Aveyard, B. P. Binks, and J. H. Clint. Emulsions stabilised solely by colloidal particles. *Adv. Colloid Interface Sci.*, **100**:503–546, 2003.
- [57] S. Arditty, C. P. Whitby, B. P. Binks, V. Schmitt, and F. Leal-Calderon. Some general features of limited coalescence in solid-stabilized emulsions. *Eur. Phys. J. E*, **11**(3):273–281, 2003.
- [58] F. Tu, B. J. Park, and D. Lee. Thermodynamically Stable Emulsions Using Janus Dumbbells as Colloid Surfactants. *Langmuir*, **29**(41):12679–12687, 2013.
- [59] C. Casagrande and M. Veyssie. Janus beads-realization and 1st observation of interfacial properties. *CR Acad. Sci. Ser. II*, **306**(20):1423–1425, 1988.
- [60] B. P. Binks and P. D. I. Fletcher. Particles adsorbed at the oil-water interface: A theoretical comparison between spheres of uniform wettability and “Janus” particles. *Langmuir*, **17**(16):4708–4710, 2001.
- [61] N. Glaser, D. J. Adams, A. Boeker, and G. Krausch. Janus particles at liquid-liquid interfaces. *Langmuir*, **22**(12):5227–5229, 2006.
- [62] C. Casagrande, P. Fabre, E. Raphael, and M. Veyssie. “Janus beads”: realization and behaviour at water/oil interfaces. *Europhys. Lett.*, **9**(3):251–255, 1989.
- [63] R. Aveyard. Can Janus particles give thermodynamically stable Pickering emulsions? *Soft Matter*, **8**(19):5233–5240, 2012.
- [64] A. Walther, M. Hoffmann, and A. H. E. Mueller. Emulsion polymerization using Janus particles as stabilizers. *Angew. Chem.-Int. Edit.*, **47**(4):711–714, 2008.
- [65] J. W. Kim, J. Cho, J. Cho, B. J. Park, Y.-J. Kim, K.-H. Choi, and J. W. Kim. Synthesis of Monodisperse Bi-Compartmentalized Amphiphilic Janus Microparticles for Tailored Assembly at the Oil-Water Interface. *Angew. Chem.-Int. Edit.*, **55**(14):4509–4513, 2016.
- [66] S. Fujii, Y. Yokoyama, Y. Miyanari, T. Shiono, M. Ito, S. Yusa, and Y. Nakamura. Micrometer-Sized Gold-Silica Janus Particles as Particulate Emulsifiers. *Langmuir*, **29**(18):5457–5465, 2013.
- [67] J. Faria, M. P. Ruiz, and D. E. Resasco. Phase-Selective Catalysis in Emulsions Stabilized by Janus Silica-Nanoparticles. *Adv. Synth. Catal.*, **352**(14-15):2359–2364, 2010.

References

- [68] S. Komura. Mesoscale structures in microemulsions. *J. Phys.-Condes. Matter*, **19**(46):463101, 2007.
- [69] G. Gompper and M. Schick. *Self-assembling amphiphilic systems, in Phase Transitions and critical phenomena, Vol. 16: C. Domb and J. L. Lebowitz eds.* Academic Press, 1994.
- [70] J. He, M. J. Hourwitz, Y. Liu, M. T. Perez, and Z. Nie. One-pot facile synthesis of Janus particles with tailored shape and functionality. *Chem. Commun.*, **47**(46):12450–12452, 2011.
- [71] F. Tu and D. Lee. Shape-Changing and Amphiphilicity-Reversing Janus Particles with pH-Responsive Surfactant Properties. *J. Am. Chem. Soc.*, **136**(28):9999–10006, 2014.
- [72] E. Passas-Lagos and F. Schueth. Amphiphilic Pickering Emulsifiers Based on Mushroom-Type Janus Particles. *Langmuir*, **31**(28):7749–7757, 2015.
- [73] S. Jiang, Q. Chen, M. Tripathy, E. Luijten, K. S. Schweizer, and S. Granick. Janus Particle Synthesis and Assembly. *Adv. Mater.*, **22**(10):1060–1071, 2010.
- [74] D. Wu, J. W. Chew, and A. Honciuc. Polarity Reversal in Homologous Series of Surfactant-Free Janus Nanoparticles: Toward the Next Generation of Amphiphiles. *Langmuir*, **32**(25):6376–6386, 2016.
- [75] C. H. J. Evers, J. A. Luiken, P. G. Bolhuis, and W. K. Kegel. Self-assembly of microcapsules via colloidal bond hybridization and anisotropy. *Nature*, **534**(7607):364–398, 2016.
- [76] G. D. Moon, T. I. Lee, B. Kim, G.S. Chae, J. Kim, S.H. Kim, J.-M. Myoung, and U. Jeong. Assembled Monolayers of Hydrophilic Particles on Water Surfaces. *ACS Nano*, **5**(11):8600–8612, 2011.
- [77] J. P. K. Seville, C. D. Willett, and P. C. Knight. Interparticle forces in fluidisation: a review. *Powder Technol.*, **113**(3):261–268, 2000.
- [78] E. Koos and N. Willenbacher. Capillary Forces in Suspension Rheology. *Science*, **331**(6019):897–900, 2011.
- [79] S. Herminghaus. Dynamics of wet granular matter. *Adv. Phys.*, **54**(3):221–261, 2005.
- [80] C. Goegelein, M. Brinkmann, M. Schroeter, and S. Herminghaus. Controlling the Formation of Capillary Bridges in Binary Liquid Mixtures. *Langmuir*, **26**(22):17184–17189, 2010.

References

- [81] S. Zeppieri, J. Rodriguez, and A. L. L. de Ramos. Interfacial tension of alkane plus water systems. *J. Chem. Eng. Data*, **46**(5):1086–1088, 2001.
- [82] W. L. Miller and A. Cacciuto. Hierarchical self-assembly of asymmetric amphiphatic spherical colloidal particles. *Phys. Rev. E*, **80**(2):021404, 2009.
- [83] B. J. Park, T. Brugarolas, and D. Lee. Janus particles at an oil-water interface. *Soft Matter*, **7**(14):6413–6417, 2011.
- [84] Y. Hirose, S. Komura, and Y. Nonomura. Adsorption of Janus particles to curved interfaces. *J. Chem. Phys.*, **127**(5):054707, 2007.
- [85] A. B. Pawar and I. Kretzschmar. Patchy particles by glancing angle deposition. *Langmuir*, **24**(2):355–358, 2008.
- [86] A. B. Pawar and I. Kretzschmar. Multifunctional Patchy Particles by Glancing Angle Deposition. *Langmuir*, **25**(16):9057–9063, 2009.
- [87] Q. Chen, E. Diesel, J. K. Whitmer, S. C. Bae, E. Luijten, and S. Granick. Triblock Colloids for Directed Self-Assembly. *J. Am. Chem. Soc.*, **133**(20):7725–7727, 2011.
- [88] G. M. Dougherty, K. A. Rose, J. B. H. Tok, S. S. Pannu, F. Y. S. Chuang, M. Y. Sha, G. Chakarova, and S. G. Penn. The zeta potential of surface-functionalized metallic nanorod particles in aqueous solution. *Electrophoresis*, **29**(5):1131–1139, 2008.